Bi-allelic *ACBD6* variants lead to a neurodevelopmental syndrome with progressive and complex movement disorders

Rauan Kaiyrzhanov,[1,†] Aboulfazl Rad,[2,3,†] Sheng-Jia Lin,[4,†] Aida Bertoli-Avella,[5,†] Wouter W. Kallemeijn,[6,7,†] Annie Godwin,[8,†] Maha S. Zaki,[9] Kevin Huang,[4] Tracy Lau,[1] Cassidy Petree,[4] Stephanie Efthymiou,[1] Ehsan Ghayoor Karimiani,[10,11] Maja Hempel,[12,13] Elizabeth A. Normand,[14] Sabine Rudnik-Schöneborn,[15] Ulrich A. Schatz,[15,16] Marc P. Baggelaar,[6,17] Muhammad Ilyas,[18,19] Tipu Sultan,[20] Javeria Raza Alvi,[20] Manizha Ganieva,[21] Ben Fowler,[22] Ruxandra Aanicai,[5] Gulsen Akay Tayfun,[23] Abdulaziz Al Saman,[24] Abdulrahman Alswaid,[25] Nafise Amiri,[26] Nilufar Asilova,[21] Vorasuk Shotelersuk,[27] Patra Yeetong,[28] Matloob Azam,[29] Meisam Babaei,[30] Gholamreza Bahrami Monajemi,[31] Pouria Mohammadi,[32,33] Saeed Samie,[31] Selina Husna Banu,[34] Jorge Pinto Basto,[5] Fanny Kortüm,[12] Mislen Bauer,[35] Peter Bauer,[5] Christian Beetz,[5] Masoud Garshasbi,[33] Awatif Hameed Issa,[36] Wafaa Eyaid,[37] Hind Ahmed,[37] Narges Hashemi,[38] Kazem Hassanpour,[39] Isabella Herman,[40,41,42,43] Sherozjon Ibrohimov,[21] Ban A. Abdul-Majeed,[44] Maria Imdad,[45] Maksudjon Isrofilov,[21] Qassem Kaiyal,[46] Suliman Khan,[5] Brian Kirmse,[47] Janet Koster,[48] Charles Marques Lourenço,[49] Tadahiro Mitani,[41] Oana Moldovan,[50] David Murphy,[51] Maryam Najafi,[52,53] Davut Pehlivan,[40,41] Maria Eugenia Rocha,[5] Vincenzo Salpietro,[1] Miriam Schmidts,[52,53,54] Adel Shalata,[55,56] Mohammad Mahroum,[54] Jawabreh Kassem Talbeya,[55,57] Robert W. Taylor,[58,59] Dayana Vazquez,[35] Annalisa Vetro,[60] Hans R. Waterham,[48] Mashaya Zaman,[34] Tina A. Schrader,[61] Wendy K. Chung,[62,63] Renzo Guerrini,[60,64] James R. Lupski,[41,42,65] Joseph Gleeson,[66,67] Mohnish Suri,[68] Yalda Jamshidi,[10,69] Kailash P. Bhatia,[51] Barbara Vona,[3,70,71] Michael Schrader,[61] Mariasavina Severino,[72] Matthew Guille,[8,‡] Edward W. Tate,[6,7,‡] Gaurav K. Varshney,[4,‡] Henry Houlden[1,‡] and Reza Maroofian[1,‡]

[†,‡]**These authors contributed equally to this work.**

Abstract

The acyl-CoA-binding domain-containing protein 6 (ACBD6) is ubiquitously expressed, plays a role in the acylation of lipids and proteins, and regulates the *N*-myristoylation of proteins via *N*-myristoyltransferase enzymes (NMTs). However, its precise function in cells is still unclear, as is the consequence of *ACBD6* defects on human pathophysiology. Utilizing exome sequencing and extensive international data sharing efforts, we identified 45 affected individuals from 28 unrelated families (consanguinity 93%) with bi-allelic pathogenic, predominantly loss-of-function (18/20) variants in *ACBD6*. We generated zebrafish and *Xenopus tropicalis acbd6* knockouts by CRISPR/Cas9 and characterized the role of *ACBD6* on protein *N*-myristoylation with YnMyr chemical proteomics in the model organisms and human cells, with the latter also being subjected further to ACBD6 peroxisomal localization studies. The affected individuals (23 males and 22 females), with ages ranging from 1 to 50 years old, typically present with a complex and progressive disease involving moderate-to-severe global developmental delay/intellectual disability (100%) with significant expressive language impairment (98%), movement disorders (97%), facial dysmorphism (95%), and mild cerebellar ataxia (85%) associated with gait impairment (94%), limb spasticity/hypertonia (76%), oculomotor (71%) and behavioural abnormalities (65%), overweight (59%), microcephaly (39%) and epilepsy (33%). The most conspicuous and common movement disorder was dystonia (94%), frequently leading to early-onset progressive postural deformities (97%), limb dystonia (55%), and cervical dystonia (31%). A jerky tremor in the upper limbs (63%), a mild head tremor (59%), parkinsonism/hypokinesia developing with advancing age (32%), and simple motor and vocal tics were among other frequent movement disorders. Midline brain malformations including corpus callosum abnormalities (70%), hypoplasia/agenesis of the anterior commissure (66%), short midbrain and small inferior cerebellar vermis (38% each), as well as hypertrophy of the clava (24%) were common neuroimaging findings. *acbd6*-deficient zebrafish and *Xenopus* models effectively recapitulated many clinical phenotypes reported in patients including movement disorders, progressive neuromotor impairment, seizures, microcephaly, craniofacial dysmorphism, and midbrain defects accompanied by developmental delay with increased mortality over time. Unlike ACBD5, ACBD6 did not show a peroxisomal localisation and ACBD6-deficiency was not associated with altered peroxisomal parameters in patient

fibroblasts. Significant differences in YnMyr-labelling were observed for 68 co- and 18 post-translationally *N*-myristoylated proteins in patient-derived fibroblasts. *N*-Myristoylation was similarly affected in *acbd6*-deficient zebrafish and *Xenopus tropicalis* models, including Fus, Marcks, and Chchd-related proteins implicated in neurological diseases. The present study provides evidence that bi-allelic pathogenic variants in *ACBD6* lead to a distinct neurodevelopmental syndrome accompanied by complex and progressive cognitive and movement disorders.

Author affiliations:

1 Department of Neuromuscular diseases, UCL Institute of Neurology, WC1N 3BG, London, UK

2 Cellular and Molecular Research Center, Sabzevar University of Medical Sciences, Sabzevar 009851, Iran

3 Tübingen Hearing Research Centre, Department of Otolaryngology, Head and Neck Surgery, Eberhard Karls University, 72076, Tübingen, Germany

4 Genes & Human Disease Research Program, Oklahoma Medical Research Foundation, Oklahoma City, OK, 73104, USA

5 CENTOGENE GmbH, 18055, Rostock, Germany

6 Department of Chemistry, Imperial College London, Molecular Sciences Research Hub, London, W12 0BZ, UK

7 The Francis Crick Institute, London, NW1 1AT, UK

8 European Xenopus Resource Centre - XenMD, School of Biological Sciences, University of Portsmouth, PO1 2DT, UK.

9 Clinical Genetics Department, Human Genetics and Genome Research Institute, National Research Centre, 12622, Cairo, Egypt

10 Genetics Research Centre, Molecular and Clinical Sciences Institute, St George's University of London, SW17 0RE, London, UK

11 Department of Medical Genetics, Next Generation Genetic Polyclinic, Mashhad, Iran

12 Institute of Human Genetics, University Medical Center Hamburg-Eppendorf, 20246, Hamburg, Germany

13 Institute of Human Genetics, University Hospital Heidelberg, Heidelberg, 69120, Germany

14 GeneDx, Gaithersburg, 20877, Maryland, USA

15 Institute of Human Genetics, Medical University Innsbruck, 6020, Austria

16 Institute of Human Genetics, Technical University of Munich, 81675, Germany

17 Utrecht University, Biomolecular Mass Spectrometry & Proteomics Group, 3584 CH Utrecht, The Netherlands

18 Department of BioEngineering, University of Engineering and Applied Sciences, 19130, Swat, Pakistan

19 Centre for Omic Sciences, Islamia College University, 25000, Peshawar, Pakistan

20 Department of Pediatric Neurology, Institute of Child Health, Children Hospital, Lahore, Pakistan

21 Department of Neurology, Avicenna Tajik State Medical University, 734063, Dushanbe, Tajikistan

22 Imaging Core, Oklahoma Medical Research Foundation, Oklahoma City, OK, 73104, USA

23 Department of Pediatric Genetics, Marmara University Medical School, 34722, Istanbul, Turkey

24 Pediatric Neurology Department, National Neuroscience Institute, King Fahad Medical City, 49046, Riyadh, Saudi Arabia

25 King Saud Bin Abdulaziz University For Health Sciences, Department of Pediatrics, King Abdullah Specialized Children's Hospital, Riyadh, Saudi Arabia

26 International Collaboration on Repair Discoveries (ICORD), University of British Columbia, V5Z 1M9, Vancouver, Canada

27 Center of Excellence for Medical Genomics, Department of Pediatrics, King Chulalongkorn Memorial Hospital, Faculty of Medicine, Chulalongkorn University, Bangkok 10330, Thailand

28 Division of Human Genetics, Department of Botany, Faculty of Science, Chulalongkorn University, Bangkok 10330, Thailand

29 Pediatrics and Child Neurology, Wah Medical College, 47000, Wah Cantt, Pakistan

30 Department of Pediatrics, North Khorasan University of Medical Sciences, Bojnurd, Iran

31 Pars Advanced and Minimally Invasive Medical Manners Research Center, Pars Hospital, 1415944911, Tehran, Iran

32 Children's Medical Center, Pediatrics Center of Excellence, Ataxia Clinic, Tehran University of Medical Sciences, Tehran, Iran

33 Faculty of Medical Sciences, Department of Medical Genetics, Tarbiat Modares University, Tehran, Iran

34 Department of Paediatric Neurology and Development, Dr. M.R. Khan Shishu (Children) Hospital and Institute of Child health, Mirpur, Dhaka- 1216, Bangladesh

35 Division of Clinical Genetics and Metabolism, Nicklas Children's Hospital, Miami, Florida, FL 33155, USA

36 University of Basrah, 61004, Basrah, Iraq

37 Department of genetics and precision medicine, King Abdullah International Medical Research Centre, King Saud bin Abdulaziz University for Health Science, King Abdulaziz Medical City, Ministry of National Guard-Health Affairs (NGHA), Riyadh, Saudi Arabia

38 Department of Pediatrics, school of Medicine, Mashhad University of Medical Sciences, 13131 – 99137, Mashhad, Iran

39 Non-Communicable Diseases Research Center, Sabzevar University of Medical Sciences, 319, Sabzevar, Iran

40 Section of Pediatric Neurology and Developmental Neuroscience, Department of Pediatrics, Baylor College of Medicine, 68010, Houston, TX, USA

41 Department of Molecular and Human Genetics, Baylor College of Medicine, TX 77030 Houston, TX, USA

42 Texas Children's Hospital, Houston, TX 77030, TX, USA

43 Pediatric Neurology, Neurogenetics and Rare Diseases, Boys Town National Research Hospital, 68131, Boys Town, NE, USA

44 Molecular Pathology and Genetics, The Pioneer Molecular Pathology Lab, Baghdad, Iraq

45 Centre for Human Genetics, Hazara University, 21300, Mansehra, Pakistan

46 Department of Pediatric Neurology, Clalit Health Care, 2510500, Haifa, Israel

47 University of Mississippi Medical Center, 2500, MS 39216, USA

48 Laboratory Genetic Metabolic Diseases, Amsterdam University Medical Centers location AMC, 1100 DD, Amsterdam, The Netherlands

49 Faculdade de Medicina, Centro Universitario Estácio de Ribeirão Preto, Ribeirão Preto, 14096-160, São Paulo, Brazil

50 Serviço de Genética Médica, Departamento de Pediatria, Hospital de Santa Maria, Centro Hospitalar Universitário de Lisboa Norte, 1649-035, Lisboa, Portugal

51 Department of Clinical and Movement Neurosciences, UCL Queen Square Institute of Neurology, University College London, WC1N 3BG, London, UK

52 Pediatrics Genetics Division, Center for Pediatrics and Adolescent Medicine, Faculty of Medicine, Freiburg University, 79106 Freiburg, Germany

53 Genome Research Divisio, Human Genetics Department, Radboud University Medical Center, 6500 HB, Nijmegen, The Netherlands

54 CIBSS-Centre for Integrative Biological Signalling Studies, University of Freiburg, Freiburg, Germany

55 Pediatrics and Medical Genetics, the Simon Winter Institute for Human Genetics, Bnai Zion Medical Center, 31048, Haifa, Israel

56 Bruce Rappaport Faculty of Medicine, the Technion institution of Technology, 3200003, Haifa, Israel

57 Department of Radiology, The Bnai Zion Medical Center, Haifa, Israel

58 Wellcome Centre for Mitochondrial Research, Translational and Clinical Research Institute, Faculty of Medical Sciences, Newcastle University, Newcastle upon Tyne, NE2 4HH, UK

59 NHS Highly Specialised Service for Rare Mitochondrial Disorders, Newcastle upon Tyne Hospitals NHS Foundation Trust, Newcastle upon Tyne, NE1 4LP, UK

60 Neuroscience Department, Meyer Children's Hospital IRCCS, 50139 Florence, Italy

61 Department of Biosciences, University of Exeter, EX4 4QD, Exeter, UK

62 Department of Pediatrics, Columbia University Irving Medical Center,

New York, NY 10032, USA

63 Department of Medicine, Columbia University Irving Medical Center, New York, NY 10032, USA

64 University of Florence, 50139 Florence, Italy

65 Human Genome Sequencing Center, Baylor College of Medicine, Houston, Texas, 77030, USA

66 Department of Neurosciences, University of California, San Diego, La Jolla, CA, 92093, USA

67 Rady Children's Institute for Genomic Medicine, San Diego, CA, 92025, USA

68 Clinical Genetics Service, Nottingham University Hospitals NHS Trust, NG5 1PB, Nottingham, UK

69 Human Genetics Centre of Excellence, Novo Nordisk Research Centre Oxford, Oxford, UK

70 Institute of Human Genetics, University Medical Center Göttingen, 37073, Göttingen, Germany

71 Institute for Auditory Neuroscience and Inner EarLab, University Medical Center Göttingen, 37075, Göttingen, Germany

72 Neuroradiology Unit, IRCCS Istituto Giannina Gaslini, 16147, Genoa, Italy

Correspondence to: Reza Maroofian

Department of Neuromuscular Disorders, UCL Queen Square Institute of Neurology, London, WC1N 3BG, UK

E-mail: r.maroofian@ucl.ac.uk

Correspondence may also be address to: Gaurav K. Varshney

Genes & Human Disease Research Program, Oklahoma Medical Research Foundation, Oklahoma City, OK, USA

E-mail: gaurav-varshney@omrf.org

Running title: *ACBD6*-related disease

Keywords: *ACBD6*; neurodegeneration; dystonia; ataxia; parkinsonism; *N*-myristoylation

Abbreviations: ACBDs=Acyl-CoA binding domain containing proteins; LCACoA=long-chain fatty acyl-CoA esters; ACBD6=Acyl-CoA-binding domain-containing protein 6; ACBD5=Acyl-CoA-binding domain-containing protein 5; ACB=Acyl-CoA binding; ANK=ankyrin repeat domain; dpf=days post-fertilization; hpf=hours post-fertilization; NMT=*N*-myristoyltransferase; Myr-CoA=myristoyl co-enzyme A; LOF=loss-of-function; PTZ=pentylenetetrazole; VSR=visual startle response; WES=whole exome sequencing; WISH=whole-mount in situ hybridization; YnMyr=myristic acid alkyne; CRISPR =Clustered Regularly Interspaced Short Palindromic Repeats GDD=global developmental delay; ID=intellectual disability

Introduction

Acyl-CoA-binding domain-containing proteins (ACBDs) are a large multigene family of intracellular lipid-binding proteins, and in mammals, they include ACBD1-7. These proteins specifically bind long-chain fatty acyl-CoA esters (LCACoA) and control their intracellular concentration.[1,2] Various cellular functions have been ascribed to this protein family, ranging from lipid homeostasis, organelle formation, apoptotic responses, intracellular vesicle trafficking, as well as tethering between the peroxisome and endoplasmic reticulum.[2] ACBDs have been suggested to play a crucial role in brain development, via their strong proliferative

effects on the neural stem and progenitor cells.[3] To date, defects in only two members of ACBDs have been associated with Mendelian disorders in humans. *ACBD5* deficiency has been reported to cause a combination of retinal dystrophy with leukodystrophy and defects in peroxisomal very long-chain fatty acid metabolism in four families.[4-7] *ACBD6* has been suggested as a candidate gene for intellectual disability (ID) in two large-cohort gene discovery studies reporting limited phenotypic data[8,9] and in a case report describing 2 siblings with neurodevelopmental disorder, obesity, pancytopenia, diabetes mellitus, cirrhosis, and renal failure but with a limited neurological phenotype.[10]

The ACBD6 protein has two domains: the N-terminal Acyl-CoA-binding (ACB) and the specialized C-terminal ankyrin repeat (ANK) domain. This protein is detected in the cytosol and nuclei of cells and modulates the acylation of lipids and proteins.[11] It has also been suggested that ACBD6 is associated with *N*-myristoyltransferase enzymes (NMTs) in human cells by ligand binding and protein interaction, although direct evidence for this in cells is lacking.[12] In humans, NMT1 and NMT2 enzymatically catalyze the *N*-myristoylation of substrate proteins by transferring the myristate from myristoyl coenzyme A (Myr-CoA) onto the N-terminal glycine of nascent proteins (co-translationally, at the ribosome) or to internal glycines uncovered by protease cleavages during apoptosis (post-translationally).[13] The global *N*-myristoylated proteome consists of more than 200 co- and post-translationally *N*-myristoylated proteins in humans,[14,15] and *N*-myristoylation is important for the association of substrates with membranes and their interaction with other proteins.[16]

Here, we describe 45 affected individuals from 28 unrelated families with 18 bi-allelic predicted loss-of-function (LOF), 1 missense, and 1 in-frame insertion variants in *ACBD6* presenting a new and distinct neurodevelopmental syndrome with a complex and progressive movement disorder phenotype. We performed functional studies in zebrafish and *Xenopus tropicalis* (*X. tropicalis*) knockouts generated by CRISPR/Cas9 that recapitulate many clinical features reported in patients. We ruled out a major role for *ACBD6* in peroxisomes and investigated the deregulation of co- and post-translationally *N*-myristoylated proteins in *ACBD6* deficient human, zebrafish, and *X. tropicalis* cells, given its putative role in modulating NMT activity.

Materials and methods

Patient identification and deep phenotyping

By using the GeneMatcher platform,[17] extensive international data sharing, and screening the variant databases of several research and diagnostic laboratories worldwide, we identified 27 families with bi-allelic variants in *ACBD6*. Follow-up details were obtained in the family reported by Yeetong *et al.* (2023).[10] For a comprehensive phenotypic characterization of the affected individuals, we obtained clinical details, including neurological examination, via a universally-adopted proforma (Supplementary Table 1). Where possible, video recordings and facial photographs of the affected individuals along with their brain MRIs were made available for review by a movement disorders specialist (K.B.), dysmorphologist (M.S.), and neuroradiologist (M.Sev.), respectively. Parents and legal guardians of all affected individuals consented to the publication of clinical and genetic information, including video and photographs, according to the Declaration of Helsinki, and the study was approved by the respective local Ethics Committees.

Genetic analysis

Using genomic DNA from whole blood samples of the probands from the 28 unrelated families, whole-exome sequencing (WES) was performed at 10 different centres worldwide with methods specified in Supplementary Table 1. WES data analysis and variant filtering and prioritization were performed using in-house implemented pipelines at different centres (Supplementary Table 1 for methods). Genotyping and homozygosity mapping were done in families 1, 3, 5, 7, and 21 according to standard procedures using the Automap software (https://automap.iob.ch/). Sanger sequencing was performed to confirm co-segregation in all available family members. mRNA expression analysis for *ACBD6* was performed by relative real-time PCR (Supplementary Method 1). RNA studies to assay the effect of the splice acceptor site variants were performed as previously described[18,19] (Supplementary Methods 2).

Functional studies in Zebrafish

Zebrafish (*Danio rerio*) were raised and maintained under standard conditions in an AALAC accredited facility at the Oklahoma Medical Research Foundation (OMRF). All experiments were performed as per protocol 22-18 approved by the Institutional Animal Care Committee of OMRF (IACUC). Wild-type zebrafish strain (*NHGRI-1*)[20] or transgenic lines as described were used for all experiments. Detailed experimental procedures are described in Supplementary Method 3.

Functional studies in *Xenopus tropicalis*

X. tropicalis was used to test the gene-disease link for *ACBD6* further in a second animal model. The details of *X. tropicalis* care, generating F0 *acbd6* crispant animals, and phenotypic analysis of F0 *acbd6* crispant animals are provided in Supplementary Methods 4. All procedures were conducted in accordance with the Home Office Code of Practice, under PP4353452 with approval from the University of Portsmouth's Animal Welfare and Ethical Review Body.

Cell culture

Human fibroblasts were obtained from skin biopsies of two unrelated affected individuals, F1:S1 and F2:S1 with a single base change in *ACBD6* affecting the splice acceptor site in intron 5 and a frameshift variant c.82dupG; p.(Val28GlyfsTer6), respectively. A control cell line from the unaffected sibling from F1 (a homozygous wild-type sibling) was established (control 1). Wild-type human control (C109) skin fibroblasts were provided by H. Waterham (control 2). COS-7 cells were cultured to perform immunofluorescence and microscopy analysis of ACBD6 localization (Supplementary Methods 5).

Analysis of peroxisomal VLCFA β-oxidation parameters

A D3-C22:0 loading test was performed by loading cells for 3 days with 30 µM deuterated (D3) C22:0 followed by fatty acid analysis with tandem mass spectrometry, essentially as previously described.[21]

YnMyr chemical proteomics, whole proteome analysis, and meta-analyses

Wild-type and ACBD6 deficient human fibroblasts, zebrafish, and *X. tropicalis* embryos were metabolically labelled in the presence or absence of YnMyr, followed by unbiased whole proteome analysis or chemical proteomics after YnMyr-enrichment to identify and quantify proteins *N*-myristoylated with YnMyr. Sample preparation, processing, and data analyses were performed as described previously, including the calculation of FDR adjusted P-values.[22,23] Meta-analysis for pathway- and disease-enrichment analysis were performed in Metacore (Clarivate). Detailed experimental procedures are described in Supplementary Methods 6.

Acbd6 expression studies in mouse brain

Gene expression in the adult mouse brain was performed and visualized as described in Supplementary Method 7.

Results

Using WES and homozygosity mapping, we identified 20 homozygous variants in *ACBD6* across 28 unrelated families. Variants were subjected to familial segregation testing (Fig. 1A) and assessed using *in silico* analysis tools and genomic databases (Table 1 and Supplementary Tables 1 and 2). All variants are listed using the canonical transcript NM_032360.4 (Fig. 1B). Family 1 showed a splice variant (c.574-2A>G) which has been shown to result in cryptic splice activation after 5 nucleotides in exon 6 (r.574_578del, p.(Arg193SerfsTer7) (Fig. 1C,

Supplementary Fig. 1)). Families 12 (c.694+1G>A) and 13 (c.664-2A>G) each harboured novel splice variants that resulted in skipping of exon 7, leading to a frameshift and premature termination (r.664_694del, p.(Asp222ProfsTer10). The (c.694+1G>A) variant showed additional evidence of activation of a cryptic splice donor site, also causing a frameshift and premature termination (r.694_694+1ins23, p.(Ala232AspfsTer8) (Fig. 1C, Supplementary Figure 2). Families 7 and 27, 8, 14, and 28 carried homozygous frameshift variants including c.474delA, p.(Asp159ThrfsTer16) (Families 7 and 27 shared this *ACBD6* variant); c.285delA, p.(Lys95AsnfsTer23); c.719_723delTTGTA, p.(Ile240ArgfsTer9); and c.360dupA, p.(Leu121ThrfsTer27), respectively. Families 2 and 21 shared the same homozygous frameshift *ACBD6* c.82dupG, p.(Val28GlyfsTer6) variant, as is the case with families 3, 16, and 17, who harboured the same homozygous frameshift *ACBD6* c.484_488delATATT, p.(Ile162Ter) variant. Families 4, 9, 11, 18, 20, 22, and 26 carried homozygous nonsense variants including c.760C>T, p.(Arg254Ter); c.594G>A, p.(Trp198Ter); c.539C>A, p.(Ser180Ter); c.217A>T, p.(Lys73Ter); c.160C>T, p.(Gln54Ter); c.280 C>T, p.(Gln94Ter); and c.216C>A, p.(Tyr72Ter), respectively. Families 5 and 15 shared the same homozygous nonsense *ACBD6* c.187G>T, p.(Glu63Ter) variant. Likewise, families 20 and 25 shared the same homozygous nonsense *ACBD6* c.160C>T, p.(Gln54Ter) variant. Families 23 and 24 each harboured a large deletion variant (c.664-18556_694+8366del, p.(?)) which spans 26,953bp of the *ACBD6* sequence and includes the complete deletion of exon 7. The affected individuals in family 6 carried an in-frame duplication variant c.654_656dupTAA, p.(Asn219dup) in exon 6. Families 10 and 19 harboured the same homozygous predicted-deleterious missense *ACBD6* variant c.602A>G, p.(Asp201Gly) in exon 6 (Fig. 1D). All variants were ultra-rare or absent in ~1.8 million alleles inspected through a number of large genetic variant databases listed in Supplementary Table 2. A detailed description of the variants is provided in Supplementary Tables 1 and 2.

Clinical delineation of *ACBD6*-related disease

The cohort includes 23 male and 22 female affected individuals whose current ages widely range between 1 and 50 years. While almost half of the individuals (21/45) were <10 years old (the 1st age group), 11/45 (25%) individuals were between the ages of 10-19 years (the 2nd age group), and 13/45 (29%) affected individuals were ≥20 years old (the 3rd age group) at the most recent

review. Two siblings from Family 28 died at the ages of 31 and 30 due to stage 5 chronic renal disease and aspiration, respectively. Almost all affected individuals are from consanguineous unions with diverse ethnic backgrounds populating South and Central Asia, the greater Middle East, Europe, and North and South America. Table 1 and Fig. 2A-D provide a summary of the core phenotypic features of 45 affected individuals from 28 unrelated families with bi-allelic *ACBD6* variants. A detailed phenotypic description is provided in Supplementary Table 1 and Supplementary case reports. Video recordings are available from 16 families (Supplementary videos 1-16).

Prenatal history was mostly unremarkable in the cohort and most of the affected individuals reached normal gestational age. Head circumference at birth was $\leq 3^{nd}$ percentile in 7/21 (33%) affected individuals. Head circumference on the latest available review was $\leq$ the 2^{nd} percentile in 12/31 (39%) individuals and height was mostly below the age-adjusted average in the cohort (18/32, 56%). Current weight was > the 50^{th} percentile in 20/34 (59%) affected individuals. All patients manifested a moderate-to-severe global developmental delay (GDD) involving all domains but predominantly affecting cognitive function and the acquisition of independent walking and expressive language. While 10 patients had failed to acquire independent ambulation by a mean age of 9.4±5.0 years (age range 4-20), the mean age of independent walking for the rest of the cohort was 3.7±1.7 years (age range 1.5-8).

Upon the latest available follow-up, moderate-to-severe GDD/ID (45/45, 100%) with significant expressive language impairment (40/41, 98% from non-verbal to a few words), movement disorders (33/34, 97%), facial dysmorphism (38/40, 95%), and mild cerebellar ataxia (35/41, 85%) associated with limb spasticity/hypertonia (31/41, 76%) and gait abnormalities (33/35, 94%) were among the cardinal clinical features observed in the *ACBD6* cohort (Fig. 2C).

The most conspicuous and common movement disorder present in all the 3 age groups was dystonia (30/32, 94%). This was frequently truncal dystonia leading to abnormal thoracic and/or thoracolumbar spinal flexion (camptocormia) (30/31, 97%) and mild-to-moderate lateral flexion of the trunk (Pisa syndrome, 22/32, 69%). Although the stooping of the body and its lateral flexion were equally common in the 2^{nd} (9/9 and 8/9, respectively) and the 3^{rd} (10/10 and 10/10, respectively) age groups, and were frequent in the 1^{st} age group (10/12 and 4/12, respectively), the severity of truncal dystonia suggested an age-dependent progression (Fig. 2B). Additionally,

some affected individuals developed mild upper limb action-induced dystonia (6/15, 40%), lower limb dystonia (12/22, 55%), and cervical dystonia (8/26, 31%).

Another common hyperkinetic movement disorder in the cohort was a tremor. The upper limb jerky tremor at rest and/or intention tremor was present in 22/35 (63%) affected individuals and 16/27 (59%) individuals had a mild head tremor. Dystonic head tremor, jerky tremor involving all limbs, and negative myoclonus were also seen in a small number of patients. With advancing age, parkinsonism/hypokinesia developed in 10/31 (32%) individuals, 6 of whom were over the age of 20 years, and 4 cases were between ages 10-20 years. A trial of levodopa was done in only 2 affected individuals with a minimal response. No other antiparkinsonian or anti dystonic medication has been tried in the cohort. Additionally, subtle perioral muscle twitching and stereotypic mouth dyskinesia were observed in the available video recordings of younger affected individuals. Remarkably, simple motor and vocal tics and tic-like vocalizations were detected in the video recordings of 7 young and adult cases (Supplementary Videos). Regarding eye movements, limited upgaze (12/26, 46%), impaired saccades (9/19, 47%), and strabismus (8/20, 40%) were frequent oculomotor abnormalities.

Lower limb spasticity, ascertained in 27/35 (77%) affected individuals, in combination with cerebellar ataxia led to gait abnormalities described as a spastic-ataxic gait in 14 patients, and clumsy/slow/broad-based or unstable gait in 17 individuals. Upper limb ataxia and spasticity were confirmed in 13 and 9 affected individuals, respectively. Tendon release surgery was done in 3 cohort members due to lower limb spasticity. Lower limb hypotonia was detected in single isolated cases.

A deterioration in motor and cognitive abilities was reported in 28/28 (100%) affected individuals suggesting a progressive disease course and underlying neurodegeneration. The oldest member of the cohort, currently aged 50 years, has lost his ability to walk independently and currently uses a wheelchair.

Complex partial, myoclonic, atonic, and generalized tonic-clonic seizures were reported in 13/39 (33%) patients with the seizure debut from neonatal age to 35 years old. Seizures were often controlled with a combination of antiepileptic medications.

Younger affected individuals were reported to have hand stereotypies, and hyperactivity was present in 9/21 (43%) patients. Signs of premature aging were seen in 9/38 (24%) individuals

from five families. Forty-six percent of patients had autistic features (13/28), temper tantrums 16/36 (44%), and aggressive behaviour (13/37, 35%) with a tendency to self-injury (6/34, 18%) were reported. Sleep disturbances (15/33, 45%) were common, and urinary incontinence was present in 15/24 (63%) individuals aged between 3-20 years.

Facial photographs were available from 32 affected individuals from 19 families (Fig. 2A). The analysis of 19 children revealed the most frequent dysmorphic features including full nasal tip (16/19), broad chin (14/19), bi-frontal/bi-temporal narrowing (12/19), hypertelorism (11/19), up-slanting palpebral fissures (9/19), and depressed nasal bridge (9/19). Assessment of 13 adult photos showed frequent signs such as a broad chin (11/13), full nasal tip (8/13), small mouth (7/13), high nasal ridge (5/13), thin upper lip (5/13) and full lower lip (5/13) (more details in Supplementary Tables 3 and 4).

Brain MRI scans were available for neuroradiological review in 29/45 subjects. The corpus callosum was abnormal in 20/29 subjects (70%): partial or complete callosal agenesis was observed in 7 individuals, while callosal hypoplasia with prevalent involvement of the posterior sections was noted in the remaining 13 individuals. In 19/29 patients (66%), there was marked hypoplasia/agenesis of the anterior commissure. Short midbrain and small inferior cerebellar vermis were each detected in 11/29 affected individuals (38%). Mild to moderate reduction of periventricular white matter with consequent ventriculomegaly was observed in 10/29 patients (34%). In 7/29 (24%) individuals, incomplete hippocampal inversion was found. Finally, mild hypertrophy of the Clava was noted in 5/21 (24%) individuals (Fig. 2D). Only 4/29 patients (14%) had normal neuroimaging findings.

Acbd6 expression studies in mouse brain

Acbd6 is expressed in nearly all regions of the adult mouse brain profiled by single-cell RNA sequencing (Supplementary Fig. 3).

Characterization of *ACBD6* LOF using CRISPR/Cas9-mediated zebrafish mutant and F_0 knockout models

Zebrafish Acbd6 protein is highly conserved across species and displayed similar tissue-specific expressions with humans (Supplementary Fig. 4). To examine the spatiotemporal expression pattern, we performed whole-mount *in situ* hybridization (WISH) analysis and results revealed that the *acbd6* mRNA was broadly expressed at 24 hours post-fertilization (hpf) and had elevated expression levels in the central nervous system, developing eyes, otic vesicle, and trunk muscles (Fig. 3A). Using CRISPR/Cas9 technology, we generated a genetic mutant of *acbd6*, and through RT-qPCR analysis, verified a significant notable decrease in *acbd6* mRNA expression in homozygous mutants (Supplementary Fig. 5A). During early embryonic developmental stages, we did not observe any visible morphological abnormalities in homozygous mutants. However, at the 6 days post-fertilization (dpf) stage, homozygous mutants (-/-) demonstrated a minor reduction in eye size (~3%, indicated by the red line in Fig. 3B) compared to wild-type (+/+) or heterozygous (+/-) animals (Fig. 3C). There was no significant change in head size (indicated by the blue line in Fig. 3B) (Fig. 3D). The visual startle response (VSR) analysis[25] indicated that reduced eye size impacts the visual function in *acbd6* -/- mutants (Fig. 3E). Furthermore, we performed locomotion behaviour tests on mutants at 6 and 12 dpf in 10-minute intervals of light-dark cycles (Fig. 3F-K and Supplementary Fig. 5-7, and detailed descriptions in Supplementary Result 3). In general, *acbd6*-/- mutants exhibited a gradual decline in locomotor activity in dark periods (Fig. 3F, G, I, J and Supplementary Fig. 7A, B, D, E) and an exaggerated response as soon as lights are turned off at 6 dpf (Figs. 3F, H, Supplementary Fig. 5C-D and Supplementary Fig. 7A, C), suggesting a hypertonia-like or spasticity behaviour.[26] As the larvae developed further at 12 dpf, the *acbd6-/-* mutants showed an increase in distance moved after light on and multiple locomotor bursts (Fig. 3I, K, Supplementary Fig. 6C and Supplementary Fig. 7D, F), indicating light-induced seizure-like behaviour.[27] The mutants also demonstrated increased mortality and severe developmental delay, with an overall reduction in brain size and disrupted muscular phenotype (Fig. 3L, M). Histological analysis showed a reduction in brain size (Fig. 3N-W), particularly in regions such as the telencephalon, optic tectum, cerebellum, and retina (Fig. 3O-Q, Fig. 3R-T, Fig. 3U-W, Supplementary Fig. 8A-C). Furthermore, skeletal muscle fibres in *acbd6-/-* mutants displayed a disrupted phenotype, characterized by shortened and

scattered fibres and gaps (Supplementary Fig. 8D-F). Interestingly, adult *acbd6* -/- mutant survivors (Supplementary Fig. 9 and Supplementary video 17, 18) exhibited behavior resembling that of individuals with an autism spectrum disorder.[28]

To verify the specificity of the *acbd6* mutant phenotype, we utilized the F_0 knockout (also known as F_0 crispant, or simply F_0) method to induce bi-allelic mutations and observed similar morphological and molecular phenotypes in homozygous mutants and F_0 (Fig. 4A-D). We discovered that F_0 also exhibited several phenotypes previously reported in affected individuals, such as hypertelorism (Fig. 4E) and facial dysmorphism (broader chin; and wider lower jaw, Supplementary Fig. 10A-H). These phenotypes were restored upon co-injection of wild-type human mRNA, confirming the specificity of the phenotype. We also introduced the LOF p.(Glu63Ter) and missense variants p.(Asp201Gly) into *acbd6* cDNA and observed impaired protein function and failure to rescue the eye size phenotype (Fig. 4F) in F_0 knockouts. We further investigated *acbd6* F_0 behaviour in light-dark cycles at 6- and 12-dpf and observed that *acbd6* F_0 exhibited lower locomotor activity during dark periods (Fig. 4G, H) and an exaggerated response after lights off, like homozygous mutants (Fig. 4G, I, and Supplementary Fig. 11A, B). Additionally, *acbd6* F_0 exhibited light-induced seizure-like behaviour (red arrows in Fig. 4G and Supplementary Fig. 11C, D). By 12 dpf, *acbd6* F_0 demonstrated reduced locomotor activity in both light and dark periods (Supplementary Fig. 12A, B). These results suggest that *acbd6* F_0 larvae exhibit more severe abnormal locomotor behaviours than homozygous mutants. We hypothesized that the loss of *acbd6* might increase susceptibility to chemical-induced seizures, as observed in *acbd6*-/- mutants showing seizure-like behaviour.[29,30] To test this hypothesis, we exposed *acbd6* F_0 and control larvae to different doses of the anticonvulsant drug, pentylenetetrazole (PTZ), and discovered that *acbd6* F_0 larvae exhibited hyperexcited behaviour at higher doses (Fig. 4J). This suggests that downregulation of *acbd6* may contribute to the onset of epilepsy-like seizures. We examined the impact of *acbd6* F_0 on neuronal and skeletal muscle development and discovered excessive axonal arborizations (Fig. 4K-N and Supplementary Fig. 13) and progressive degeneration of muscle fibres in *acbd6* F_0 larvae (Fig. 4O-T and Supplementary Fig. 14). We also observed an increase in myelin basic protein a (*mbpa*) expression in both *acbd6* F_0 and homozygous mutant (Supplementary Fig. 15A, B), which may explain the abnormal axonal development phenotype. A detailed description of our results can be found in the Supplementary Results 2. In summary, our zebrafish model replicated many of the

clinical features seen in individuals with bi-allelic variants in *ACBD6*, highlighting how these variants may contribute to the progressive disease course. Our extensive analysis of both mutant and F_0 in *acbd6* provides insight into the underlying mechanisms of the disease observed in affected individuals.

Xenopus ACBD6 F_0 knockout models

X. tropicalis and humans have the same *acbd6* gene structures (Fig. 5A) and share 66% amino acid identity (Supplementary Fig. 16A). Crispant F_0 tadpoles were produced by injection of two non-overlapping sgRNAs targeting exon 1 of *acbd6* (Supplementary Fig. 16B). The effects were specific, since both sgRNAs produced the same phenotype and when embryos with a SNP in the PAM for one sgRNA were used, the embryos developed normally (Supplementary Fig. 17A, 3rd upper panel from the left). ICE analysis[31] of target amplicon sequences (Supplementary Fig. 16C) showed that at the gastrula stage, 74% of alleles in the embryos had indels, and that 63.5% had a frameshift from a predominant 8bp deletion (sgRNA 68). For sgRNA71 the average was a 53.6% KO from a mix of indels. The range of phenotypes at later stages was due to distinct levels of frameshift mutations among the groups (Supplementary Fig. 16D).

The first notable phenotype was gastrulation failure due to reduced cell movements (Fig. 5B and Supplementary Fig. 17A). This limits the analysis of phenotypes at later stages since the surviving embryos have been selected to have significantly greater mosaicism than normally produced in this type of experiment. At swimming tadpole stages more than half of the crispants had obvious craniofacial abnormalities (n = 36; Fig. 5C, Supplementary Fig. 17D, and Fig.17E) and head measurement showed a decrease in the average area from 2.07 +/- 0.36 mm^2 in controls to 1.52 +/- 0.27 mm^2 in crispants ($t(34)=5.183$, $p<0.001$; Fig. 5D). This was not a result of a defect in the structure of the head cartilage, although when *in situ* it did appear constrained by the overall head structure (compare Fig. 5E (control) and F (crispant)). The cartilage components were nonetheless present and morphologically normal upon dissection; however, the overall cartilage size was smaller than controls consistent with the observed microcephaly. To detect subtler changes in head structure, we compared control and crispant tadpoles by MicroCT (Fig. 5G). Three things were apparent in the three embryos selected at random from the crispant group: first, the eyes (yellow arrows) were abnormal and displaced (e.g. the dorsal and frontal

views in the right-hand panel) and in one case there was anophthalmia, the latter was rare because it was not detected in the bright field images. Second, a muscle in the face was poorly developed or absent (red arrows). From comparison with *X. laevis* staining,[32] we tentatively identified this as the geniohyoidius, although the muscle seems more distant from the midline in *X. tropicalis* than in *X. laevis*. The brain also has obvious structural abnormalities which are most pronounced in the midbrain (blue arrows). Comparing the movement of control and *acbd6* crispant tadpoles showed that the crispants move less over a 10-minute period (average 2.37 mm/s for controls and 1.01 mm/s for crispants, n = 50). The difference was statistically significant ($t(78)=4.9$, $p=<0.001$) (Fig. 5H) (Supplementary videos 19-22). After the deaths at gastrulation, crispants and control embryos survived similarly until the feeding stage (Fig. 5I).

Loss of ACBD6 does not impact peroxisome function

Several members of the ACBD family have been linked to peroxisome function.[2] Furthermore, peroxisomal dysfunction is linked to developmental defects and neurological abnormalities.[33] To investigate if peroxisomal parameters were altered in *ACBD6* deficiency, patient (from F1:S1 and F2:S1) and control (F1:II-2 unaffected sibling; wild type C109) fibroblasts were processed for immunofluorescence using antibodies against the peroxisomal membrane marker PEX14 and catalase, a peroxisomal matrix protein (Fig. 6 A, B). No alterations in peroxisome protein import, morphology, distribution, or number were observed when compared to control fibroblasts (Fig. 6 A, B). In addition, expression of a Myc-ACBD6 construct in COS-7 cells confirmed a cytoplasmic and nuclear localisation of Myc-ACBD6,[34] but did not provide evidence for a peroxisomal localisation under standard culture conditions (Fig. 6C). In addition, fatty acid analysis after a D3-C22:0 loading test in cultured fibroblasts did not reveal any abnormalities of peroxisomal VLCFA β-oxidation (Supplementary Table 5) as observed in *ACBD5* deficiency.[5,33] Detailed results are described in Supplementary Results 3.

Investigation of the effect of *ACBD6* deficiency on *N*-myristoylation in patient-derived fibroblasts

We employed a chemical proteomic approach to identify and quantify *N*-myristoylated proteins, by combining metabolic labelling of living cells with YnMyr,[14] an alkyne-containing myristic acid analogue, and Click chemistry-enabled enrichment of YnMyr-labelled proteins, coupled to mass spectrometry proteomics analysis.[22] Chemical proteomics revealed 68 known co-translationally, and 18 post-translationally *N*-myristoylated proteins expressed in the fibroblasts derived from F1:S3 and his healthy sibling (Supplementary Fig. 18A, B, respectively). As expected, the incorporation of YnMyr was markedly reduced by treatment with 100 nM IMP-1088, a selective and highly potent NMT inhibitor,[23,35] in both the fibroblasts of the healthy control and the patient, confirming the specificity of labelling (Supplementary Fig. 18C, D, respectively). Proteins co- and post-translationally *N*-myristoylated with YnMyr were detected in significantly higher abundance in the patient-derived fibroblasts compared to the healthy sibling (Supplementary Fig. 18E), suggesting ACBD6 deficiency provokes increased incorporation of YnMyr, potentially through increased *N*-myristoylation or upregulation of lipid salvage pathways leading to increased YnMyr import (Fig. 6D). We hypothesise this may be caused by the differential interplay of the two *N*-myristoyltransferases (NMT1 and NMT2) with ACBD6 for various substrates. Although fibroblasts from only one affected individual and a healthy sibling were compared, the apparent differential *N*-myristoylation warrants more detailed investigations of the role of ACBD6 in *N*-myristoylation in cell types involved in the described human clinical phenotypes.

Proteomics analyses of developing wild-type and *acbd6* crispant zebrafish

To shed light on the potential role of *acbd6* on *N*-myristoylation during zebrafish development, we employed metabolic labelling with YnMyr and chemical proteomics at different stages of development. At 72 and 120 hpf, both wild-type and *acbd6* crispant zebrafish express >32 significantly enriched proteins, for each of which the human orthologue is a validated co-translationally *N*-myristoylated substrate (Supplementary Figs. 19A-D). In addition, significantly

enriched proteins also included >48 proteins with N-terminal glycine, thereby potentially *N*-myristoylated, but where unequivocal evidence of *N*-myristoylation is currently lacking the human orthologue, or where the human orthologue does not possess an N-terminal glycine. At 72 hpf, an increased abundance of YnMyr-labelled proteins is observed in the *acbd6* crispant, including Marcks and Chchd-related proteins, known to be co-translationally *N*-myristoylated in humans (Fig. 7A). Of note, zebrafish express duplications of multiple proteins, including the aforementioned Marcks and Chchd-related proteins (Fig. 7A). Conversely, enrichment of several zebrafish proteins with N-terminal glycine in zebrafish but not found with a N-terminal glycine in humans was significantly reduced in *acbd6* crispants, including Sfpq, associated with brain development, CNS neuron axonogenesis and midbrain-hindbrain boundary initiation (Fig. 7A). Similar increases in Marcks and Chchd-related proteins are observed in the *acbd6* crispants at 120 hpf, whereas Fus and Fusl are further decreased (Fig. 7B).

We next performed a whole proteomics analysis comparing wild-type and *acbd6* crispant at 72 and 120 hpf (Supplementary Figs. 19E, F, respectively). In contrast to the significant increase of YnMyr labelling observed in *acbd6* crispants (Figure 7A, B), the abundance of *N*-myristoylated proteins such as Marcks and Chchd-related proteins is not significantly increased at the whole proteome level at 72 and 120 hpf, further indicating the role of *acbd6* on the process of *N*-myristoylation in zebrafish. Meta-analysis of up-regulated proteins in *acbd6* crispants revealed a significant involvement of translation- and metabolism-related pathways (Supplementary Fig. 20A), and significant enrichments in disease networks including frontotemporal dementia and delayed speech and language development (Supplementary Fig. 20B). Down-regulated proteins are significantly involved in pathways related to nervous system development, as well as neurodegeneration (Fig. 7C). Enriched disease-related networks include dystonia muscle spasticity and movement disorders, a striking similarity with the observations in affected individuals (Supplementary Fig. 20C). At 120 hpf, a meta-analysis of the whole proteome data reveals similar enrichments (Supplementary Fig. 20D-G). Notably, upregulated proteins enrich in translation- and metabolism-related pathways, whereas downregulated proteins further enrich in pathways of neurological development and disease, including spasticity (Supplementary Fig. 20G).

Proteomics analyses of developing wild-type and *acbd6* crispant *X. tropicalis*

Similar to the chemical proteomics analyses in zebrafish, we used YnMyr labelling to identify *N*-myristoylated substrates and the pathways affected by the loss of *acbd6* in developing *Xenopus.* Here, wild-type, crispant 68 or crispant 71 *X. tropicalis* were metabolically labelled from 1 hpf to 18 hpf, due to the previously reported growth arrest. Chemical proteomics of YnMyr labelling revealed >10 *X. tropicalis* proteins the human orthologues of which are known to be co-translationally *N*-myristoylated, including a duplication of Marcks, as well as *X. tropicalis* proteins which share the N-terminal glycine with their orthologue in humans (Supplementary Fig. 21A-C). Comparing wild-type with *acbd6* crispant 68 and 71 (Figs. 7D and E, respectively) reveals a marked depletion of YnMyr-labelled proteins in the crispants, including all identified *X. tropicalis* proteins with co-translationally *N*-myristoylated human orthologues. Both crispants reveal prominent and significant reductions in proteins including Marcks, Ppm1b, Ppm1g. Whole proteome analysis revealed Marcks and Fus are markedly reduced in *acbd6* crispant 68, while Ppm1a is slightly increased, and in *acbd6* crispant 71, both Marcks and Ppm1b are reduced (Supplementary Figs 21D, E). Meta-analysis (Supplementary Fig. 22) revealed upregulated proteins in crispants 68 and 71 are significantly affected in pathways of translation and metabolism, and notably, the 'Parkinson-disease'-specific disease network was significantly enriched (Fig. 7F).

Discussion

A neurodevelopmental syndrome with progressive movement disorders characterizes *ACBD6*-related disease

Despite their predicted roles in cellular lipid metabolism, the functions of many of the ACBDs still remain unclear, as is the consequence of ACBD protein defects on human pathophysiology. In this study, we identified novel and ultra-rare bi-allelic predicted LOF variants in *ACBD6* as the disease cause in 45 previously undiagnosed individuals from 28 unrelated families. A wide age range of the cohort members (1-50 years) delineated the age-related clinical spectrum and the natural history of the *ACBD6*-related disease. The disease had an invariably early-onset and

inevitably progressive course with significant motor and cognitive deterioration upon reaching adulthood, a course suggestive of underlying neurodegeneration. The phenotype is complex involving the constellation of extrapyramidal, pyramidal, and cerebellar ataxia symptoms associated with GDD/ID, microcephaly, and variable epilepsy. Impaired expressive language, delayed gait acquisition, and early-onset stooped posture with lateral trunk flexion (Pisa syndrome) were among the important pathognomonic features. Additionally, tics and tic-like vocalizations seen in 6 affected individuals are peculiar features associated with several neurological disorders, particularly with chorea-acanthocytosis.[36] Whilst the present cohort of patients with *ACBD6*-related disease did have facial dysmorphism, it did not suggest a recognizable facial "gestalt". The most common dysmorphic feature in the cohort was a broad chin. Of note, most of the patients had hypoplasia/agenesis of the corpus callosum and anterior commissure, suggesting a potential role for *ACBD6* in axonal pathfinding and corpus callosum development. Interestingly, claval hypertrophy observed in the present cohort is a well-documented neuroradiological sign of *PLA2G6*-associated neurodegeneration.[37]

Defects in numerous genes and pathways are known to present with the constellation of symptoms observed in *ACBD6*-related disease, particularly, with various combinations of dystonia, parkinsonism, ataxia, and spasticity.[38-41] Their clinical phenotypes are typically classified according to the predominating symptom; however, a later approach tends to define this with a spectrum of genetic dystonia-ataxia, parkinsonism-dystonia/ataxia, and ataxia-spasticity syndromes.[38-41] Thus, several forms of complicated hereditary spastic paraplegia, spastic ataxia, and young-onset dystonia-parkinsonism syndromes may overlap with *ACBD6* phenotypes. A suggested differential diagnosis with the disease pathways involved is given in Supplementary Table 7.

It has been suggested that neurodevelopmental abnormalities and neurodegeneration could share several molecular and cellular mechanisms. For instance, proteins, such as Aβ, MAPT/tau, Rac1, Progranulin, Huntingtin, PINK, and Parkin, frequently implicated in Alzheimer's disease, Parkinson’s disease, and Huntington’s diseases are important for nervous system development.[42] A wide range of multisystem genetic disorders could present with a biphasic course where complex neurological phenotype gradually evolves on the background of a pre-existing neurodevelopmental disorder.[43,44] Therefore, we propose a likely clinical continuum associated

with *ACBD6*-related disease, characterized by a combination of neurodevelopmental abnormalities and neurodegeneration.

Zebrafish *acbd6* knockouts recapitulate many features observed in affected individuals

In recent years, the zebrafish has gained significance as an animal model for investigating neurodevelopmental disorders, owing to its high physiological similarity to humans and its responsiveness to genetic and pharmacological interventions.[45,46] The acyl-CoA binding domain of human and zebrafish ACBD6 share significant identity and similarity in the ankyrin-repeat motif and acyl-CoA binding domain, with 80% identity and 95.4% similarity in the former and 69.2% identity and 78.2% similarity in the latter. Zebrafish models for ACBD proteins do not currently exist; however, by generating *acbd6* knockouts in zebrafish, we observed similar phenotypes to those of affected individuals, such as movement disorders, seizures, and facial dysmorphology. Our findings suggest that *acbd6* is critical for animal development, as the loss of this protein results in severe global developmental delay and increased mortality over time, as evidenced by stunted growth and severe brain development impairment by 30 dpf. Moreover, we observed motor neuron over-branching during development and progressive muscle loss, suggesting a combination of muscle and neuronal degeneration leading to movement abnormalities. Furthermore, the knockout zebrafish demonstrated increased locomotor behaviour in the dark, potentially indicating seizure or anxiety-like behaviour, similar to that seen in affected patients. In summary, the Acbd6 zebrafish models offer a promising tool for gaining deeper mechanistic insights into the role of *acbd6* and for screening potential therapeutic interventions, as zebrafish are ideal for high-throughput *in vivo* drug screening. As such, the *acbd6* model represents a valuable resource for drug discovery research.

X. tropicalis acbd6 knockouts have gastrulation failure, brain defects, and reduced locomotion

X. tropicalis is a diploid clawed frog with a genome that contains over 80% of identified human disease genes and importantly is syntenic with over two-thirds of the human genome.[47] Features of this animal include rapid external development and a transparent tadpole. A deep understanding of *Xenopus* biology throughout the last 70 years,[48] combined with ease of genetic manipulation[49], makes it powerful for modeling disease genes[50,51] and understanding genetic disease mechanisms.[52-55]

In the present study, the inactivation of *acbd6* in *X. tropicalis* caused severe cell movement failures during gastrulation. Marcks requires *N*-myristoylation to act in early development[56] and is required for normal cell movement during gastrulation in frog.[57] It is interesting to speculate that the loss of *acbd6* may cause gastrulation defects due to a loss of Marcks *N*-myristoylation; an aspect that requires future work. Due to embryo deaths at gastrula stages, a caveat for the interpretation of the subsequent phenotype analysis is the unusually high mosaicism of these crispant tadpoles. Despite this, there were clear phenotypic differences between the control and crispant tadpoles. In some cases, the change predominated in one-half of the tadpole due to mosaicism (on the L-R axis, see for example Fig. 5G second image from the left). These differences included microcephaly, reduced movement, eye abnormalities, and brain structure differences, data that strengthen the link between *ACBD6* variants and the pathology observed in the patient cohort.

ACBD5 and *ACBD6* have different cellular localizations but both genes exhibit a neurodegenerative phenotype

ACBD5 is a peroxisomal membrane protein. Although current knowledge of the phenotype associated with *ACBD5* defects is limited to only four reported families,[4-7] similar to *ACBD6*, individuals with defective *ACBD5* seem to exhibit a neurodegenerative disease, albeit with a different range of associated symptoms. Our study on peroxisome morphology and function with ACBD6 deficient and control fibroblasts did not reveal significant alterations as has been

demonstrated in ACBD5 deficiency. Furthermore, Myc-ACBD6 did not localize to peroxisomes when expressed in COS-7 cells.

ACBD6 deficiency alters myristate probe YnMyr incorporation into substrates of NMT

Our chemical proteomics analysis comparing *N*-myristoylated proteins in fibroblasts, derived from a patient and their healthy sibling, revealed significant differences in YnMyr-labelled proteins. YnMyr incorporation was significantly higher in the ACBD6-deficient patient fibroblasts, spanning 68 known co- and 18 post-translationally *N*-myristoylated proteins. Interestingly, an apparent differential variation of YnMyr incorporation in the identified NMT substrates between healthy and patient fibroblasts was also observed. Our investigation in *ACBD6* deficient fibroblasts might indicate its role in *N*-myristoylation of a subset of NMT substrates, but further studies are required to investigate this putative role of ACBD6. Furthermore, to study the effect of ACBD6 deficiency on *N*-myristoylation, future analyses will need to focus on cell types likely directly impacting the pathways involved in *e.g.* neurological development.

Both the zebrafish and *X. tropicalis* model systems recapitulate many of the identified human phenotypes, including movement disorders, seizures, facial dysmorphology, and developmental defects. This evidence for notable evolutionary conservation of ACBD6 function across mammals, amphibia, and teleosts emphasizes the power of multiple, non-mammalian models as a method for rapid and cost-effective human gene analysis. Through our chemical proteomics analysis, coupled with whole proteome and meta-analysis, we identified that *acbd6*-deficiency in developing zebrafish embryos results in a prominent increase in metabolic labelling of known co- and post-translationally *N*-myristoylated proteins with YnMyr, suggesting *N*-myristoylation is dependent on a direct or indirect interaction between *acbd6* and the *N*-myristoyltransferases. Meta-analysis furthermore revealed that *acbd6* deficiency provokes an overall increase of proteins *N*-myristoylated with YnMyr, with a subset involved in the development of the eye, neuron and muscle, being reduced. Overall, this suggests that *ACBD6* is involved in the *N*-myristoylation of a subset of *N*-myristoyltransferase substrates that require modification, and

might indicate activation of a rescue mechanism in response to loss of *ACBD6*. Concomitantly, potentially compromised myristic acid-CoA binding and shuttling to *N*-myristoyltransferases in ACBD6-deficient cells may upregulate salvage pathways to increase cellular myristate concentration. For example, acyl-CoA synthases can activate exogenous lipids directly, potentially bypassing or compensating loss of ACBD6. In this case, YnMyr-CoA could more effectively compete with endogenous myristic acid-CoA for protein *N*-myristoylation than in healthy subjects, leading to the observed enhanced YnMyr labelling, suggesting exogenous myristic acid supplementation through dietary supplementation might have the potential to reduce the burden of ACBD6 deficiency. The determined differences in protein *N*-myristoylation between the skin fibroblasts derived from a single patient and unaffected sibling align with the YnMyr chemical proteomics findings from our zebrafish study. Consequently, the YnMyr chemical proteomics data of the human patient and unaffected fibroblast serves only as qualitative confirmatory evidence of the zebrafish study. For this purpose, we did not seek further replication of these findings across multiple patient cell lines.

In contrast to *ACBD6* deficient human fibroblasts and zebrafish crispants, the *acbd6 X. tropicalis* crispants show a prominent and significant reduction of YnMyr labelling, including proteins such as Marcks, Chchd, Ppm1b, Ppm1g, and Fus, which are significantly involved in development. Meta-analysis indicates the upregulation of neurological and sight-related disease networks upon *acbd6* loss. The significant effect of *acbd6* loss on *X. tropicalis* development at the gastrula stage precludes a clear interpretation of the effect of *acbd6* knockout on *N*-myristoylation due to the presence of confounding changes in other processes during the period of metabolic labelling. The clearly non-viable state of the *X. tropicalis* embryos likely leads to defects in lipid metabolism, protein translation and related processes over this period which go beyond the direct impact of *acbd6* on cells.

In summary, we have shown that bi-allelic pathogenic variants in *ACBD6* are associated with a new and distinct neurodevelopmental disease with a complex and progressive dystonia-parkinsonism-ataxia phenotype. Zebrafish and *X. tropicalis* crispants recapitulate the main clinical features of the cohort with affected pathways underlying translation, metabolism, neurological development, and neurological diseases. Further studies are warranted to delineate the clinical phenotype and understand the pathomorphological presentation and molecular mechanisms of the *ACBD6*-related disease. This includes elucidating the molecular interplay

between ACBD6 and *N*-myristoyltransferases involved in the co- and post-translational modification of nascent protein chains, how ACBD6 affects lipid metabolism and the identification of treatments of ACBD6 deficiency.

Data availability

The data that support the findings of this study are available from the corresponding author, upon reasonable request. The mass spectrometry proteomics data have been deposited to the ProteomeXchange Consortium via the PRIDE[24] partner repository with the dataset identifiers PXD024957 (YnMyr chemical proteomics in human cells), PXD043676 (YnMyr chemical proteomics in zebrafish), PXD043679 (zebrafish whole proteome), PXD043677 (YnMyr chemical proteomics in X. tropicalis) and PXD043680 (X. tropicalis whole proteome).

Acknowledgements

The authors are grateful to the families for their support and consent to the publication of this study. The families were recruited as part of the SYNaPS Study Group collaboration funded by The Wellcome Trust and strategic award (Synaptopathies) funding (WT093205 MA and WT104033AIA). This research was conducted as part of the Queen Square Genomics group at University College London, supported by the National Institute for Health Research University College London Hospitals Biomedical Research Centre. We thank Prof. Zimmer, Neuroradiology Technical University of Munich for providing MRI scans. We would like to thank A. Le Quang for generation of the Myc-ACBD6 construct and J. Passmore for support with peroxisome quantification. R.G. and A.V. are members of the European Reference Networks EpiCARE and ITHACA. S. R.-S. is a member of the European Reference Network EURO NMD.

Funding

This study was funded by the MRC (MR/S01165X/1, MR/S005021/1, G0601943, MR/V012177/1), The National Institute for Health Research University College London Hospitals Biomedical Research Centre, Rosetree Trust, Ataxia UK, MSA Trust, Brain Research UK, Sparks GOSH Charity, Muscular Dystrophy UK (MDUK), Muscular Dystrophy Association (MDA USA). M.Schr. is supported by the BBSRC (BB/N01541X/1, BB/T002255/1, BB/W015420/1) and the European Union's Horizon 2020 research and innovation programme under the Marie Skłodowska-Curie grant agreement No 812968 PERICO (to M.Schr., H.W.). R.K. is supported by the Rosetrees Trust PhD Plus award (PhD2022\100042). H.H. and R.K. are supported by Global Parkinson's Genetic Program (GP2) MJFF Grant ID: MJFF-022153. B.V. is supported by Intramural Funding (fortüne) at the University of Tübingen (2545-1-0.), the Ministry of Science, Research and Art Baden-Württemberg and the German Research Foundation VO 2138/7-1 grant 469177153 as well as through the Collaborative Research Center 889 and the Multiscale Bioimaging Cluster of Excellence (MBExC). The European Commission (Marie Sklodowska Curie Individual Fellowship grant 752165 to W.W.K.), EPSRC (Impact Acceleration Account grant PS1042 to W.W.K. and E.W.T.), Cancer Research UK (C29637/A21451 and C29637/A20183 to E.W.T.). Work in the E.W.T. laboratories is supported by the Francis Crick Institute, which receives its core funding from Cancer Research UK (FC001057 and FC001097), the UK Medical Research Council (FC001057 and FC001097), and the Wellcome Trust (FC001057 and FC001097). M.Shm. acknowledges funding form the Deutsche Forschungsgemeinschaft (DFG, German Research Foundation) – Project-ID 431984000 – SFB 1453 (CRC Nephgen) and Excellence Initiative CIBSS - EXC-2189 - Project ID 390939984. R.G. is supported by the Tuscany Region Call for Health 2018 (grant DECODE-EE) and the Brain project by Fondazione CA.RI.FI. G.K.V. is supported by a grant from Oklahoma Medical Research Foundation, USA. These results reported here were generated using funding received from the Solve-RD project within the European Rare Disease Models & Mechanisms Network (RDMM-Europe). The Solve-RD project has received funding from the European Union's Horizon 2020 research and innovation programme under grant agreement No 779257 (G.K.V., R.M., H.H.). Department of Public Genetics - Israeli MOH (A.S.). Work at the EXRC is supported by the BBSRC (BB/R014841/1) and Wellcome Trust (212942/Z/18/Z).

Work in the laboratory of J.R.L. is funded in part by US National Institutes of Health (NINDS NS105078; NHGRI HG011758) and the Spastic Paraplegia Foundation. R.W.T. is funded by the Wellcome Centre for Mitochondrial Research (203105/Z/16/Z), the Mitochondrial Disease Patient Cohort (UK) (G0800674), the Medical Research Council International Centre for Genomic Medicine in Neuromuscular Disease (MR/S005021/1), the Medical Research Council (MR/W019027/1), the Lily Foundation, the Pathological Society, the UK NIHR Biomedical Research Centre for Ageing and Age-related disease award to the Newcastle upon Tyne Foundation Hospitals NHS Trust and the UK NHS Highly Specialized Service for Rare Mitochondrial Disorders of Adults and Children. V.Sh. is supported by Thailand's Health Systems Research Institute (HSRI 66-122). Y.J. is supported by Newlife Charity grant (SG/18-19/02). M.Ily. was funded through HEC-NRPU grant (17341). For the purpose of Open Access, the author has applied a CC BY public copyright license to any Author Accepted Manuscript version arising from this submission.

Competing interests

E.W.T. is a director and shareholder of Myricx Pharma Ltd, and an inventor on a patent application describing NMT inhibitors including IMP-1088 (Bell, AS; Tate, EW; Leatherbarrow, RJ; Hutton, JA; Brannigan, JA, "Compounds and their use as inhibitors of *N*-myristoyl transferase", PCT In Appl (2017) WO 2017001812). E.A.N. is an employee of GeneDx, LLC. J.R.L. holds stock in 23andMe and is a consultant for Genome International. Y.J. is an employee of Novo Nordisk.

Supplementary material

Supplementary material is available at *Brain* online.

References

1. Neess D, Bek S, Engelsby H, Gallego SF, Faergeman NJ. Long-chain acyl-CoA esters in metabolism and signaling: Role of acyl-CoA binding proteins. *Prog Lipid Res*. Jul 2015;59:1-25. doi:10.1016/j.plipres.2015.04.001

2. Islinger M, Costello JL, Kors S, *et al*. The diversity of ACBD proteins - From lipid binding to protein modulators and organelle tethers. *Biochim Biophys Acta Mol Cell Res*. May 2020;1867(5):118675. doi:10.1016/j.bbamcr.2020.118675

3. Bi J, Mischel PS. Acyl-CoA-Binding Protein Fuels Gliomagenesis. *Cell Metab*. Aug 6 2019;30(2):229-230. doi:10.1016/j.cmet.2019.07.007

4. Abu-Safieh L, Alrashed M, Anazi S, *et al*. Autozygome-guided exome sequencing in retinal dystrophy patients reveals pathogenetic mutations and novel candidate disease genes. *Genome Res*. Feb 2013;23(2):236-47. doi:10.1101/gr.144105.112

5. Bartlett M, Nasiri N, Pressman R, Bademci G, Forghani I. First reported adult patient with retinal dystrophy and leukodystrophy caused by a novel ACBD5 variant: A case report and review of literature. *Am J Med Genet A*. Apr 2021;185(4):1236-1241. doi:10.1002/ajmg.a.62073

6. Ferdinandusse S, Falkenberg KD, Koster J, *et al*. ACBD5 deficiency causes a defect in peroxisomal very long-chain fatty acid metabolism. *J Med Genet*. May 2017;54(5):330-337. doi:10.1136/jmedgenet-2016-104132

7. Gorukmez O, Havali C, Gorukmez O, Dorum S. Newly defined peroxisomal disease with novel ACBD5 mutation. *J Pediatr Endocrinol Metab*. Jan 27 2022;35(1):11-18. doi:10.1515/jpem-2020-0352

8. Najmabadi H, Hu H, Garshasbi M, *et al*. Deep sequencing reveals 50 novel genes for recessive cognitive disorders. *Nature*. Sep 21 2011;478(7367):57-63. doi:10.1038/nature10423

9. Hu H, Kahrizi K, Musante L, *et al*. Genetics of intellectual disability in consanguineous families. *Mol Psychiatry*. Jul 2019;24(7):1027-1039. doi:10.1038/s41380-017-0012-2

10. Yeetong P, Tanpowpong N, Rakwongkhachon S, Suphapeetiporn K, Shotelersuk V. Neurodevelopmental Disorder, Obesity, Pancytopenia, Diabetes Mellitus, Cirrhosis, and Renal

Failure in ACBD6-Associated Syndrome A Case Report. *Neurol-Genet.* Feb 2023;9(1)doi:ARTN e200046

10.1212/NXG.0000000000200046

11. Soupene E, Kuypers FA. Ligand binding to the ACBD6 protein regulates the acyl-CoA transferase reactions in membranes. *J Lipid Res*. Oct 2015;56(10):1961-71. doi:10.1194/jlr.M061937

12. Soupene E, Schatz UA, Rudnik-Schoneborn S, Kuypers FA. Requirement of the acyl-CoA carrier ACBD6 in myristoylation of proteins: Activation by ligand binding and protein interaction. *PLoS One*. 2020;15(2):e0229718. doi:10.1371/journal.pone.0229718

13. Losada de la Lastra A, Hassan S, Tate EW. Deconvoluting the biology and druggability of protein lipidation using chemical proteomics. *Curr Opin Chem Biol*. Feb 2021;60:97-112. doi:10.1016/j.cbpa.2020.10.002

14. Thinon E, Serwa RA, Broncel M, *et al*. Global profiling of co- and post-translationally N-myristoylated proteomes in human cells. *Nat Commun*. Sep 26 2014;5:4919. doi:10.1038/ncomms5919

15. Castrec B, Dian C, Ciccone S, *et al*. Structural and genomic decoding of human and plant myristoylomes reveals a definitive recognition pattern. *Nat Chem Biol*. Jul 2018;14(7):671-679. doi:10.1038/s41589-018-0077-5

16. Meinnel T, Dian C, Giglione C. Myristoylation, an Ancient Protein Modification Mirroring Eukaryogenesis and Evolution. *Trends in Biochemical Sciences*. Jul 2020;45(7):619-632. doi:10.1016/j.tibs.2020.03.007

17. Sobreira N, Schiettecatte F, Valle D, Hamosh A. GeneMatcher: a matching tool for connecting investigators with an interest in the same gene. *Hum Mutat*. Oct 2015;36(10):928-30. doi:10.1002/humu.22844

18. Rad A, Schade-Mann T, Gamerdinger P, *et al*. Aberrant COL11A1 splicing causes prelingual autosomal dominant nonsyndromic hearing loss in the DFNA37 locus. *Hum Mutat*. Jan 2021;42(1):25-30. doi:10.1002/humu.24136

19. Tompson SW, Young TL. Assaying the Effects of Splice Site Variants by Exon Trapping in a Mammalian Cell Line. *Bio Protoc*. May 20 2017;7(10)doi:10.21769/BioProtoc.2281

20. LaFave MC, Varshney GK, Vemulapalli M, Mullikin JC, Burgess SM. A defined zebrafish line for high-throughput genetics and genomics: NHGRI-1. *Genetics*. Sep 2014;198(1):167-70. doi:10.1534/genetics.114.166769

21. van de Beek MC, Dijkstra IM, Kemp S. Method for Measurement of Peroxisomal Very Long-Chain Fatty Acid Beta-Oxidation and De Novo C26:0 Synthesis Activity in Living Cells Using Stable-Isotope Labeled Docosanoic Acid. *Methods Mol Biol*. 2017;1595:45-54. doi:10.1007/978-1-4939-6937-1_5

22. Kallemeijn WW, Lanyon-Hogg T, Panyain N, *et al*. Proteome-wide analysis of protein lipidation using chemical probes: in-gel fluorescence visualization, identification and quantification of N-myristoylation, N- and S-acylation, O-cholesterylation, S-farnesylation and S-geranylgeranylation. *Nat Protoc*. Nov 2021;16(11):5083-5122. doi:10.1038/s41596-021-00601-6

23. Kallemeijn WW, Lueg GA, Faronato M, *et al*. Validation and Invalidation of Chemical Probes for the Human N-myristoyltransferases. *Cell Chem Biol*. Jun 20 2019;26(6):892-900 e4. doi:10.1016/j.chembiol.2019.03.006

24. Perez-Riverol Y, Csordas A, Bai J, *et al*. The PRIDE database and related tools and resources in 2019: improving support for quantification data. *Nucleic Acids Res*. Jan 8 2019;47(D1):D442-D450. doi:10.1093/nar/gky1106

25. Scott CA, Marsden AN, Slusarski DC. Automated, high-throughput, in vivo analysis of visual function using the zebrafish. *Dev Dyn*. May 2016;245(5):605-13. doi:10.1002/dvdy.24398

26. Kurolap A, Kreuder F, Gonzaga-Jauregui C, *et al.* Bi-allelic variants in neuronal cell adhesion molecule cause a neurodevelopmental disorder characterized by developmental delay, hypotonia, neuropathy/spasticity. *Am J Hum Genet.* Mar 3 2022;109(3):518-532. doi:10.1016/j.ajhg.2022.01.004

27. Eimon PM, Ghannad-Rezaie M, De Rienzo G, *et al.* Brain activity patterns in high-throughput electrophysiology screen predict both drug efficacies and side effects. *Nat Commun*. Jan 15 2018;9(1):219. doi:10.1038/s41467-017-02404-4

28. Rea V, Van Raay TJ. Using Zebrafish to Model Autism Spectrum Disorder: A Comparison of ASD Risk Genes Between Zebrafish and Their Mammalian Counterparts. *Front Mol Neurosci*. 2020;13:575575. doi:10.3389/fnmol.2020.575575

29. Basnet RM, Zizioli D, Taweedet S, Finazzi D, Memo M. Zebrafish Larvae as a Behavioral Model in Neuropharmacology. *Biomedicines*. Mar 26 2019;7(1)doi:10.3390/biomedicines7010023

30. Bertoncello KT, Bonan CD. Zebrafish as a tool for the discovery of anticonvulsant compounds from botanical constituents. *Eur J Pharmacol*. Oct 5 2021;908:174342. doi:10.1016/j.ejphar.2021.174342

31. Conant D, Hsiau T, Rossi N, *et al*. Inference of CRISPR Edits from Sanger Trace Data. *CRISPR J*. Feb 2022;5(1):123-130. doi:10.1089/crispr.2021.0113

32. Ziermann JM, Diogo R. Cranial muscle development in frogs with different developmental modes: direct development versus biphasic development. *J Morphol*. Apr 2014;275(4):398-413. doi:10.1002/jmor.20223

33. Berger J, Dorninger F, Forss-Petter S, Kunze M. Peroxisomes in brain development and function. *Biochim Biophys Acta*. May 2016;1863(5):934-55. doi:10.1016/j.bbamcr.2015.12.005

34. Soupene E, Serikov V, Kuypers FA. Characterization of an acyl-coenzyme A binding protein predominantly expressed in human primitive progenitor cells. *J Lipid Res*. May 2008;49(5):1103-12. doi:10.1194/jlr.M800007-JLR200

35. Mousnier A, Bell AS, Swieboda DP, *et al*. Fragment-derived inhibitors of human N-myristoyltransferase block capsid assembly and replication of the common cold virus. *Nat Chem*. Jun 2018;10(6):599-606. doi:10.1038/s41557-018-0039-2

36. Mainka T, Balint B, Govert F, *et al*. The spectrum of involuntary vocalizations in humans: A video atlas. *Mov Disord*. Dec 2019;34(12):1774-1791. doi:10.1002/mds.27855

37. Singh S, Mishra SC, Israrahmed A, Lal H. Typical MRI features of PLA2G6 mutation-related phospholipase-associated neurodegeneration (PLAN)/infantile neuroaxonal dystrophy (INAD). *BMJ Case Rep*. Mar 25 2021;14(3)doi:10.1136/bcr-2021-242586

38. Franco G, Lazzeri G, Di Fonzo A. Parkinsonism and ataxia. *J Neurol Sci*. Feb 15 2022;433:120020. doi:10.1016/j.jns.2021.120020

39. Morales-Briceno H, Fung VSC, Bhatia KP, Balint B. Parkinsonism and dystonia: Clinical spectrum and diagnostic clues. *J Neurol Sci*. Feb 15 2022;433:120016. doi:10.1016/j.jns.2021.120016

40. Rossi M, Balint B, Millar Vernetti P, Bhatia KP, Merello M. Genetic Dystonia-ataxia Syndromes: Clinical Spectrum, Diagnostic Approach, and Treatment Options. *Mov Disord Clin Pract*. Jul-Aug 2018;5(4):373-382. doi:10.1002/mdc3.12635

41. Synofzik M, Schule R. Overcoming the divide between ataxias and spastic paraplegias: Shared phenotypes, genes, and pathways. *Mov Disord*. Mar 2017;32(3):332-345. doi:10.1002/mds.26944

42. Schor NF, Bianchi DW. Neurodevelopmental Clues to Neurodegeneration. *Pediatr Neurol*. Oct 2021;123:67-76. doi:10.1016/j.pediatrneurol.2021.07.012

43. Deneubourg C, Ramm M, Smith LJ, *et al*. The spectrum of neurodevelopmental, neuromuscular and neurodegenerative disorders due to defective autophagy. *Autophagy*. Mar 4 2022;18(3):496-517. doi:10.1080/15548627.2021.1943177

44. Leuzzi V, Nardecchia F, Pons R, Galosi S. Parkinsonism in children: Clinical classification and etiological spectrum. *Parkinsonism Relat D*. Jan 2021;82:150-157. doi:10.1016/j.parkreldis.2020.10.002

45. Sakai C, Ijaz S, Hoffman EJ. Zebrafish Models of Neurodevelopmental Disorders: Past, Present, and Future. *Front Mol Neurosci*. 2018;11:294. doi:10.3389/fnmol.2018.00294

46. Varshney GK, Sood R, Burgess SM. Understanding and Editing the Zebrafish Genome. *Adv Genet*. 2015;92:1-52. doi:10.1016/bs.adgen.2015.09.002

47. Hellsten U, Harland RM, Gilchrist MJ, *et al*. The genome of the Western clawed frog Xenopus tropicalis. *Science*. Apr 30 2010;328(5978):633-6. doi:10.1126/science.1183670

48. De Robertis EM, Gurdon JB. A Brief History of Xenopus in Biology. *Cold Spring Harb Protoc*. Dec 1 2021;2021(12)doi:10.1101/pdb.top107615

49. Nakayama T, Blitz IL, Fish MB, *et al.* Cas9-based genome editing in Xenopus tropicalis. *Methods Enzymol*. 2014;546:355-75. doi:10.1016/B978-0-12-801185-0.00017-9

50. Ismail V, Zachariassen LG, Godwin A, *et al.* Identification and functional evaluation of GRIA1 missense and truncation variants in individuals with ID: An emerging neurodevelopmental syndrome. *Am J Hum Genet.* Jul 7 2022;109(7):1217-1241. doi:10.1016/j.ajhg.2022.05.009

51. Naert T, Van Nieuwenhuysen T, Vleminckx K. TALENs and CRISPR/Cas9 fuel genetically engineered clinically relevant Xenopus tropicalis tumor models. *Genesis*. Jan 2017;55(1-2)doi:10.1002/dvg.23005

52. Barbosa S, Greville-Heygate S, Bonnet M, *et al.* Opposite Modulation of RAC1 by Mutations in TRIO Is Associated with Distinct, Domain-Specific Neurodevelopmental Disorders. *Am J Hum Genet*. Mar 5 2020;106(3):338-355. doi:10.1016/j.ajhg.2020.01.018

53. Macken WL, Godwin A, Wheway G, *et al.* Biallelic variants in COPB1 cause a novel, severe intellectual disability syndrome with cataracts and variable microcephaly. *Genome Med*. Feb 25 2021;13(1):34. doi:10.1186/s13073-021-00850-w

54. Willsey HR, Exner CRT, Xu Y, *et al.* Parallel in vivo analysis of large-effect autism genes implicates cortical neurogenesis and estrogen in risk and resilience. *Neuron*. Mar 3 2021;109(5):788-804 e8. doi:10.1016/j.neuron.2021.01.002

55. Nakayama T, Fisher M, Nakajima K, *et al.* Xenopus pax6 mutants affect eye development and other organ systems, and have phenotypic similarities to human aniridia patients. *Dev Biol.* Dec 15 2015;408(2):328-44. doi:10.1016/j.ydbio.2015.02.012

56. Swierczynski SL, Siddhanti SR, Tuttle JS, Blackshear PJ. Nonmyristoylated MARCKS complements some but not all of the developmental defects associated with MARCKS deficiency in mice. *Dev Biol.* Oct 10 1996;179(1):135-47. doi:10.1006/dbio.1996.0246

57. Iioka H, Ueno N, Kinoshita N. Essential role of MARCKS in cortical actin dynamics during gastrulation movements. *J Cell Biol.* Jan 19 2004;164(2):169-74. doi:10.1083/jcb.200310027

Figure legends

Figure 1 Family pedigrees, schematic variants' representation, conserved regions of substitution variants in *ACBD6*, and splicing effects. (A) Pedigrees and segregation results for the 28 unrelated families. Double lines between individuals represent consanguinity. The 45 affected individuals recruited for the study are shaded and indicated with their respective subject (S) number (S1, S2 or S3). The segregation data for all individuals tested via Sanger sequencing is shown with the presence of the *ACBD6* variant (red) and/or the reference allele (black), two red/black texts indicate a homozygous state, and one red + one black text indicates a heterozygous state. The genotyping is based on the coding DNA sequence. WT refers to wild type, DEL refers to deletion and DUP refers to duplication. **(B)** Schematic representation of the gene and protein positions of detected variants in *ACBD6*. *ACBD6* is located on chromosome 1 at cytogenetic position q25.2q25.3 (upper panel). The middle panel shows the genetic variants mapped to the NM_032360.4 transcript of *ACBD6*. The lower panel shows *ACBD6* variants mapped on the protein level. Three variants including p.(Gly22fs), p.(Leu121ThrfsTer27), and a 30kb deletion in the C-terminus have been reported previously.[6, 7,10] Recurrent variants are lebelled by family codes. **(C)** Splicing schematic for the c.574-2A>G variant in *ACBD6* showing cryptic acceptor splice site activation in exon 6 (upper panel). The c.664-2A>G (middle panel) and c.694+1G>A (lower panel) variants affect splicing of exon 7 both show exon skipping. Additionally, the c.694+1G>A variant activates a cryptic donor splice site. **(D)** Interspecies alignment performed with Clustal Omega showing the complete conservation down to invertebrates of the amino acid residues affected by a missense variant leading to an amino acid substitution p.(Asp201Gly) and an in-frame duplication p.(Asn219dup).

Figure 2 Clinical features of the affected individuals with bi-allelic *ACBD6* variants. (A) i-xiii: Representative photographs demonstrating facial features of the affected individuals in adulthood. F1:S1 (i), F1:S2 (ii), F1:S3 (iii), F3:S2 (iv), F3:S1 (v), F6:S1 (vi), F7:S2 (vii), F7:S1 (viii), F11:S1 (ix), F17:S1 (x), F17:S2 (xi), F20:S1 (xii), F16:S1 (xiii). xiv-xxxi: Representative photographs demonstrating facial features of the affected individuals in childhood. F3:S2 (xiv) at 5 years old, F3:S1 (xv) at 12 years old, F6:S2 (xvi), F8:S1 (xvii), F8:S2 (xviii), F10:S1 (xix), F10:S2 (xx), and F11:S1 (xxi) at younger age, F13:S1 (xxii), F14:S1 (xxiii), F15:S1 (xxiv),

F16:S1 (xxv) at 2 years old, F16:S1(xxvi) at 4 years old, F19:S1 (xxvii), F19:S2 (xxviii), F20:S2 (xxix), F12:S1 (xxx), F12:S2 (xxxi). The most frequently seen facial dysmorphologies in adults are high nasal ridge, full nasal tip, small mouth, thin upper lip, and broad chin. The most frequently seen facial dysmorphologies in children are bi-frontal/bi-temporal narrowing, arched eyebrows, hypertelorism, up-slanting palpebral fissures, depressed nasal bridge, full nasal tip, thin upper lip, full lower lip, and broad chin. **(B)** Representative photographs demonstrating postural abnormalities seen in the affected individuals. A stooped body posture and lateral flexion of the trunk can be seen in the individuals including F1:S1 (i), F1:S2 (ii), F1:S3 (iii), F3:S1 (iv), F3:S2 (v), F6:S1 (vi), F6:S2 (vii), and F8:S2 (viii), F13:S1 (ix). **(C)** Bar graph summarizing proportions of various clinical findings in the *ACBD6* cohort. Blue – affected, orange – unaffected, grey – not ascertained/not applicable. GDD, Global developmental delay. ID, Intellectual disability. **(D)** Representative neuroimaging features of the affected individuals. Brain MRI, midline sagittal images of the affected individuals F1:S1 (i), F1:S2 (ii), F5:S1(iii), F56:S2 (iv), F7:S1 (v), F7:S2 (vi), F10:S1 (vii), F10:S2 (viii), F11:S1 (ix), F13:S1 (x), F14:S1 (xi), and F19:S1 (xii). Most of the affected individuals have corpus callosum agenesis or hypoplasia with prevalent involvement of the posterior sections (empty arrows), variably associated with short midbrain (thin arrows) and small inferior cerebellar vermis (arrowheads). In addition, mild hypertrophy of the clava was noted in some subjects (dotted arrows). Note that the anterior commissure was markedly hypoplastic or absent in all affected individuals.

Figure 3 CRISPR/Cas9 mutation of zebrafish *acbd6* causes smaller eyes, impaired vision, abnormal locomotion, developmental delay, and increased mortality. (A) Whole-mount *in situ* hybridization for detecting *acbd6* mRNA expression pattern in zebrafish embryo at 24 hpf. Forebrain (fb), midbrain (mb), midbrain and hindbrain boundary (MHB), hindbrain (hb), otic vesicle (ov). Dorsal view, anterior to the left. **(B)** Representative images of wild-type (*acbd6*+/+), heterozygous (*acbd6*+/-) and homozygous (*acbd6*-/-) mutant larva at 6 dpf. Head size and eye size are indicated by blue and red lines, respectively. Anterior to the left and dorsal to the top. Scale bar = 200 μm. **(C, D)** Quantification of eye and head size as indicated in Fig. 3B. +/+ (n = 26 larvae), +/- (n = 114 larvae) and -/- (n = 47 larvae). Each symbol represents one larva. Values are calculated as a percentage of the mean value of +/+ larvae. Error bars = mean ±

standard deviation (SD). **(E)** The result of VSR analysis performed on +/+ (n = 43 larvae), +/- (n = 99 larvae), and -/- (n = 48 larvae) zebrafish larvae at 6 dpf. Each symbol represents one larva. The number of responses for 5 stimuli of each larva is calculated as a percentage of responses. Error bars = mean ± standard error of the mean (SEM). **(F)** Locomotor activities of zebrafish larvae in light and dark periods at 6 dpf. +/+ (n = 42 larvae), +/- (n = 99 larvae), and -/- (n = 48 larvae) zebrafish larvae were habituated in the dark for 30 minutes, followed by three cycles of 10-minute time bins of light and dark periods. Error bars = mean ± SEM. The dark period (D) and light period (L) are labelled. Black arrows indicate the increased movement of homozygous mutants at the first minute in the dark. **(G)** Average cumulative distance traveled of each larva from three cycles of either light or dark periods in Fig. 3F. Error bars = mean ± SD. **(H)** Average cumulative distance traveled of each larva during the first minute of the dark period across three cycles as indicated by black arrows in Fig. 3F. Error bars = mean ± SD. **(I)** Locomotor activities of zebrafish larvae in light and dark conditions at 12 dpf. +/+ (n = 39 larvae), +/- (n = 71 larvae) and -/- (n = 29 larvae). Error bars = mean ± SEM. Red arrow indicates increased movement of homozygous mutants at the first minute after light on. Red arrowhead indicates increased movement of homozygous mutants at the second minute after light on. **(J)** Average cumulative distance traveled by each larva during three cycles of either light or dark periods in Fig. 3I. Error bars = mean ± SD. **(K)** Average cumulative distance traveled by each larva during the first cycle of the first minute of the light period as indicated by red arrow in Fig. 3I. Error bars = mean ± SD. **(L)** Genotyping results of zebrafish at 6 dpf (n = 191 larvae), 12 dpf (n = 196 larvae) and 30 dpf (n = 118 juveniles) stages from *acbd6*+/- intercross. **(M)** Representative images of morphological phenotype from *acbd6*+/+, *acbd6*+/- and *acbd6*-/- at 30 dpf. Anterior to the left and dorsal to the top. **(N)** Sagittal section of *acbd6*+/+ brain at 30 dpf. Anterior to the left and dorsal to the top. Olfactory bulb (Ob), periventricular gray zone of optic tectum (PGZ), medulla oblongata (MO). **(O-W)** Representative images of transverse sections of telencephalon (O-Q), optic tectum (R-T) and cerebellum (U-W) from *acbd6*+/+, *acbd6*+/- and *acbd6*-/- juvenile as indicated in Fig. 3N. In (C, D), one-way ANOVA with Tukey's multiple comparisons test. In (E, G, H, J, K), one-way ANOVA with Dunnett's T3 multiple comparisons test. ns, not significant $p \geq 0.05$, *$p < 0.05$, **$p < 0.01$, ***$p < 0.001$ and ****$p < 0.0001$.

Figure 4 Zebrafish *acbd6* F_0 knockouts exhibit increased susceptibility to chemical-induced seizures, excessive motor neuron branching, and skeletal muscle degeneration. (A) Representative images of uninjected control and *acbd6* F_0 larvae at 6 dpf. Left column, ventral view, anterior to the left. Right column, dorsal view, anterior to the left. Blue line indicates head size, magenta line indicates eye size, and cyan line indicates eye distance. Scale bar = 0.2 mm. **(B, C)** Quantification of the head and eye size (n = 30 larvae for each group) of uninjected control (uninj.), *acbd6* F_0 knockout (F_0), F_0 + zebrafish wild-type *acbd6* mRNA (+acbd6), and F_0 + human wild-type *ACBD6* mRNA (+ACBD6) as indicate in Fig. 4B. **(D)** The VSR analysis after mRNA rescue at 6 dpf. n = 36 larvae for each group. Each symbol represents one larva. The number of responses to 5 stimuli of each larva was calculated as a percentage of responses. Error bars = mean ± SEM. **(E)** Quantification of the eyes distance (n = 20 larvae for each group) as indicate in Fig. 4B. **(F)** Quantification of the eye size of F_0 knockout rescued with mRNA of human p.Glu63Ter (+E63*) or p.Asp201Gly (+D201G) variant. n = 25 larvae for each group. **(G)** Locomotor activities of zebrafish larvae in light and dark conditions at 6 dpf. n = 64 larvae for each group. The larvae were habituated in the dark for 30 minutes, followed by three cycles of 10-minute periods of light and dark. Error bars represent the mean ± SEM. Dark period (D), light period (L). Red arrows indicating increased movement of F_0 one minute after light on, and black arrows indicate increased movement one minute after light off. **(H)** Average cumulative distance traveled by each larva during three cycles of either light or dark periods in Fig. 4G. Error bars = mean ± SD. **(I)** The average cumulative distance traveled by each larva during the first minute of the dark period was measured over three cycles, as shown by the black arrow in Fig. 4G. Error bars represent the mean ± SD. **(J)** The average cumulative distance traveled by the larvae was measured for each group after being treated with different doses of pentylenetetrazole (PTZ) at 5 dpf. n = 16 larvae for each group**. (K-N)** Confocal images of *Tg(mnx1:GFP;olig2:DsRed)* larva at 12 dpf are shown, with transgenic larvae injected with *slc45a2* sgRNA used as a control and those injected with *acbd6* + *slc45a2* sgRNAs shown as *acbd6* F_0. (L' and N') Enlarged images from white boxes are shown in L' and N', with red asterisks indicating autofluorescence from remaining pigment cells. GFP and DsRed are displayed in cyan and magenta, respectively, with magenta arrowheads indicating excess axonal arborizations. The images are presented in a lateral view, with anterior to the left and dorsal to the top. Additional motor neuron phenotypes at 6 and 12 dpf can be found in Supplementary Fig.

13. **(O-T)** Confocal images of stained skeletal muscle fibers with phalloidin are presented, including images from *slc45a2* sgRNA-injected control (O-Q) and *acbd6* + *slc45a2* sgRNAs-injected (R-S) larvae at 12 dpf. Orthogonal views generated from (P and S) using the Orthogonal views tool in ImageJ are also displayed. Degenerated muscles are indicated by (#), while white arrowheads and a white arrow indicate Z-discs and the thickness of the myotube, respectively. Supplementary Fig. 14 provides additional muscle phenotypes at 6 and 12 dpf. In (B-D and F), one-way ANOVA with Tukey's multiple comparisons test. In (E and H-J), one-way ANOVA with Dunnett's T3 multiple comparisons test. ns, not significant $p \geq 0.05$, *$p < 0.05$, **$p < 0.01$, ***$p < 0.001$ and ****$p < 0.0001$.

Figure 5 *acbd6 X. tropicalis* crispants have gastrulation, movement, craniofacial, brain and eye defects together with microcephaly. (A) The gene structure of human (*ACBD6*) and *X .tropicalis* (*acbd6*) reveals 8 exons. **(B)** Gastrulation defects, including failure of blastopore closure and anterior posterior defects, were observed in F_0 *X. tropicalis* embryos injected with two different CRISPR/Cas9 constructs (sgRNA-68 and sgRNA-71) disrupting exon 1 of *acbd6*. **(C)** Those animals surviving to free-feeding stages presented with microcephaly, craniofacial dysmorphism and eye abnormalities. **(D)** The differences in head size between the uninjected control (2.07 +/- 0.36mm) and *acbd6* crispant tadpoles (1.52 +/- 0.27mm, sgRNA-68) were found to be significant, $t(34)=5.183$, $p<0.001$. (E-F) Alcian Blue staining marking the cartilaginous structures in the head and neck show equivalent structures between control **(E)** and *acbd6* crispant tadpoles **(F)** revealing no gross morphological abnormalities. **(G)** Detailed structural analysis in higher resolution MicroCT imaging (1% phosphotungstic acid contrast stain) revealed significant structural abnormalities in the facial musculature (Red arrows, G), abnormalities of the eye (microphthalmia, anophthalmia – Yellow arrows, G) and structural abnormalities in the brain most pronounced in the midbrain regions (Blue arrow, G). **(H)** Locomotion analysis at NF44/45 revealed that crispants moved significantly less than control tadpoles. **(I)** The Kaplan-Meier survival analysis of 65 control and crispant tadpoles shows two periods of crispant-specific decline, the first at gastrula stages (day 0-1) and the second with post-feeding (day 8, NF stage 47).

Figure 6 Morphological characteristics of peroxisomes in *ACBD6*-deficient patient cells are not altered and chemical proteomic profiling of *N*-myristoylation in human fibroblasts. (A) Patient fibroblasts and controls were processed for immunofluorescence microscopy using antibodies against the peroxisomal membrane marker PEX14, the matrix marker catalase, or mitochondrial ATP synthetase B (ATPB). Peroxisomal localisation of PEX14 and catalase indicate that peroxisomal membrane and PTS1-dependent matrix import are normal. Note that the morphology of mitochondria, which are elongated in fibroblasts, was also not altered when compared to controls. **(B)** Quantification of peroxisome number based on immunofluorescence images (see A for representative images) (n = 29-36 cells). Data are from three independent experiments. ns, not significant; Kruskal-Wallis ANOVA test with Dunn's multiple comparisons. **(C)** COS-7 cells were transfected with plasmids encoding Myc-ACBD5 or Myc-ACBD6 and processed for immunofluorescence microscopy using antibodies against Myc and PEX14. Note that Myc-ACBD5 localises to peroxisomes, whereas Myc-ACBD6 localises to the nucleus and the cytoplasm in COS-7 cells. Scale bars, 10 µm. **(D)** Ranked plot of YnMyr-labelled, known co- and post-translationally *N*-myristoylated proteins, as identified in (Supplementary Figure 18E). Position on the left equals lower abundance in ACBD6 deficient fibroblasts, position on the right equals higher abundance in ACBD6 deficient fibroblasts.

Figure 7 Chemical and whole proteome analysis of *acbd6* wild-type and crispant zebrafish and *X. tropicalis* model systems. (**A**) Volcano plot comparing YnMyr labelling of proteins in wild-type and *acbd6* crispant zebrafish at 72 hpf. Horizontal dotted line: significance threshold (p-value = 0.05). FC: fold-change. Position on the left equals reduced in crispant, position on the right equals increased in crispant. (**B**) Comparing YnMyr labelling of proteins in wild-type and *acbd6* crispant zebrafish at 120 hpf. Further description as in (A). (**C**) Top-20 of biological processes most significantly enriched in proteins down-regulated in *acbd6* crispant zebrafish at 72 hpf. The most significantly enriched process at the top. Colour indicates Q-value as secondary significance indicator. Size of circles indicates a number of proteins enriched in the depicted process. Dr: Danio rerio. Hs: Homo sapiens. (**D**) Volcano plot comparing YnMyr labelling of proteins in wild-type and *acbd6* crispant 68 *X. tropicalis*. Horizontal dotted line: significance threshold (p-value = 0.05). FC: fold-change. Position on the left equals reduced in crispant, position on the right equals increased in crispant. (**E**) Comparing YnMyr labelling of proteins in

wild-type and *acbd6* crispant 71 *X. tropicalis.* Further description as in (D). (**F**) Top-20 of biological processes most significantly enriched in proteins up-regulated in *acbd6* crispant 68 *X. tropicalis*. Most significantly enriched processes are at the top. Colour indicates Q-value as secondary significance indicator. Size of circles indicates a number of proteins enriched in the depicted process. Xt: *Xenopus tropicalis*. Hs: Homo sapiens.

Table 1 Main clinical features of the affected individuals with homozygous *ACBD6* variants

Family ID	1	2	3	4	5	6	7	8	9	10	11	12	13	14	15	16	17	18	19	20	21	22	23	24	25	26	27	28
N of affected	3	1	2	1	2	2	2	2	1	2	1	2	1	1	1	1	2	1	2	2	1	2	2	1	1	2	2	2
GDD/ID	3+	+	2+	+	2+	2+	2+	2+	+	2+	+	2+	+	+	+	+	2+	+	2+	2+	+	2+	2+	+	+	2+	2+	2+
Progressive disease course	3+	X	2+	X	2+	2+	2+	2+	X	2+	+	2X	+	+	+	X	2+	X	2X	2X	+	2X	2+	+	X	2X	2+	2+
Microcephaly	1+	-	2-	+	2-	1+	1+	2+	X	2-	-	2-	+	-	-	+	2X	-	2+	2X	-	2X	2-	+	X	2X	1+	2X
Short stature	3-	+	1+	X	2-	2+	2+	2+	-	2-	+	2-	+	+	-	X	2X	X	2-	2+	+	2X	1- = 1X	+	X	2X	2X	2X
Facial dysmorphism	3+	+	2+	X	2+	2+	2+	2+	+	2+	+	2+	+	+	+	+	2+	X	2+	2+	+	2X	2-	+	X	2X	2+	2+
Oculomotor abnormalities	3X	X	2+		2+	2+	2X	1+	X	2+	-	2+	+	-	+	+	2X	+	2-	1+	+	2X	2-	X	X	2X	2+	2X
Cerebellar ataxia	3+	+	1+	+	2+	2+	2+	2+	-	2+	+	2+	+	+	+	+	2+	X	2+	2+	-	2X	2-	-	X	2+	2+	2+
Limb spasticity/hypertonia	3+	+	2+	+	2+	1+	2+	2+	-	2+	-	2-	+/-	+	+/-	+	2+	X	2+	2-	-	2X	1+ = 1-	-	X	2+	2+	2+
Gait abnormalities	1+	+	2+	+	2+	2+	2+	2+	-	2+	+	2+	+	X	+	+	2+	+	2+	2X p	X	2X	1+ = 1X	X	X	2+	2+	2+
No independent gait	1+	+	2-	X	2-	2-	2-	2-	-	1+	-	2-	-	+	-	-	1+	-	2+	2+	+	2X	1- = 1X	+	+	2X	2-	2-
Hypokinesia/Parkinsonism	3+	X	1+	X	2-	2+	2X	2-	X	2X	X	2-	-	-	-	+	1+	X	2-	2-	-	2X	2-	-	X	2X	1+	1+
Truncal/limb dystonia	3+	X	2+	X	2+	2+	2X	2+	X	2+	+	1+ = 1-	+	+	+	+	2+	X	2+	2+	+	2X	2X	-	X	2X	2+	2+
Upper limb/head tremor	3X	+	2+	+	2+	2+	2-	2-	-	2+	+	2-	+	+	+	+	2+	+	2+	2-	-	2X	2-	-	X	2X	2+	2X
Tics and TLV	1+	X	1+	X	2X	2X	2X	2+	X	2-	-	2X	+	X	X	X	2X	-	2X	1+	-	2X	2-	-	X	2X	1+	2X
Postural instability	2+	X	2-	X	2+	2X	2X	2+	X	2+	+	2-	+	+	+	+	2X	X	2X	2X	X	2X	1- = 1X	X	X	2X	2+	2+
Epileptic seizures	2+	+	2-	+	2+	2-	2-	2-	+	2-	-	2-	+	-	-	+	2X	-	2-	2-	+	2X	1+ = 1-	-	+	2X	2-	2-
Behavioural problem	3+	-	2-	-	2+	2+	2+	2-	-	2+	-	2-	+	+	+	+	2X	X	2+	2+	-	2X	1+ = 1-	-	X	2X	2+	2+
Premature aging	3+	-	2-	-	2-	1+	1+	2-	-	2-	-	2-	-	-	-	-	2+	-	2-	2-	-	2X	2-	-	X	2X	2-	2+
Reduction of PWM	2+[a]	X	1+	X	1+	1+	1+	1-[a]	X	2+	-	2X	+	-	-	X	2X	X	2-	2-	X	2X	2X	X	X	2X	2-	2X
CC hypoplasia/agenesis	2+[a]	+	1+	X	1+	1+	2+	1-[a]	X	2+	+	2X	-	+	-	+	2+	X	2+	2-	+	2X	2X	X	X	2X	2+	2X
AC Hypoplasia/agenesis	2+[a]	X	2-	X	2+	2+	2+	1+[a]	X	2+	+	2X	+	+	+	X	2X	X	2+	2-	X	2X	2X	X	X	2X	2+	2X
Short midbrain	2+[a]	X	2-	X	1+	2+	1+	1+[a]	X	2+	+	2X	-	+	-	X	2X	X	2-	2-	X	X	2X	X	X	2X	2-	2X

ICV hypoplasia	2+[a]	X	2-	X	1+	2+	1+	1+[a]	X	1+	-	2X	+	+	-	X	2X	X	2-	2-	+	2X	2X	X	X	2X	2-	2X
Hypertrophy of the clava	2-[a]	X	2-	X	2-	1+	1-	1-[a]	X	2-	-	2X	+	+	-	X	2X	X	2+	2-	X	2X	2X	X	X	2X	2-	2X

- = negative for the feature of interest; + = positive for the feature of interest; +/- = mild hypertonia; AC = anterior commissure; CC = corpus callosum; F = family; GDD = global developmental delay; ICV = hypoplasia of the inferior cerebellar vermis; ID = intellectual disability; N = number; PWM = periventricular white matter; TLV = tic like vocalizations; X = not available/not applicable. The numbers preceding the symbols "+" = "-" = and "X" indicate the number of siblings who are positive, negative or don't have data on the feature of interest in families with multiple affected.

[a]Brain MRI scans are not available from another affected sibling.

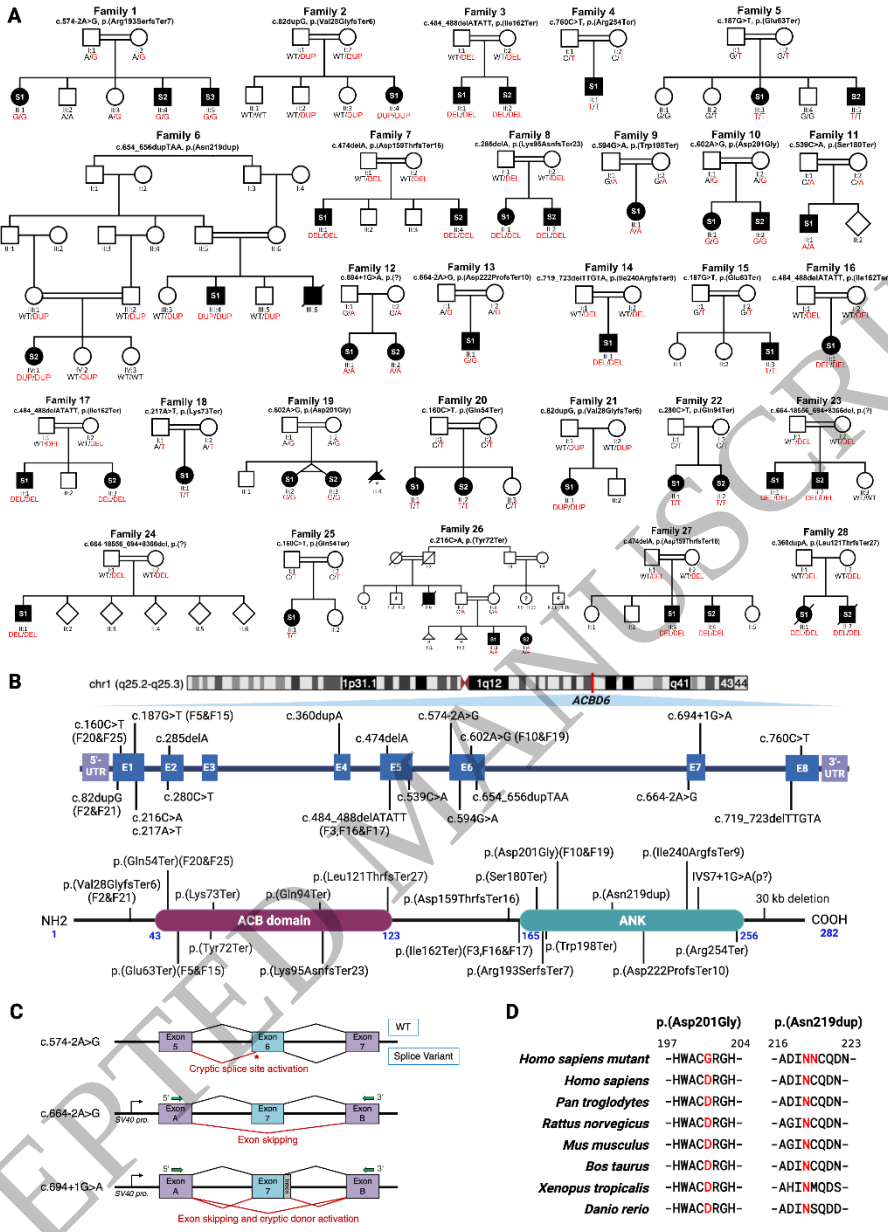

Figure 1
246x336 mm (x DPI)

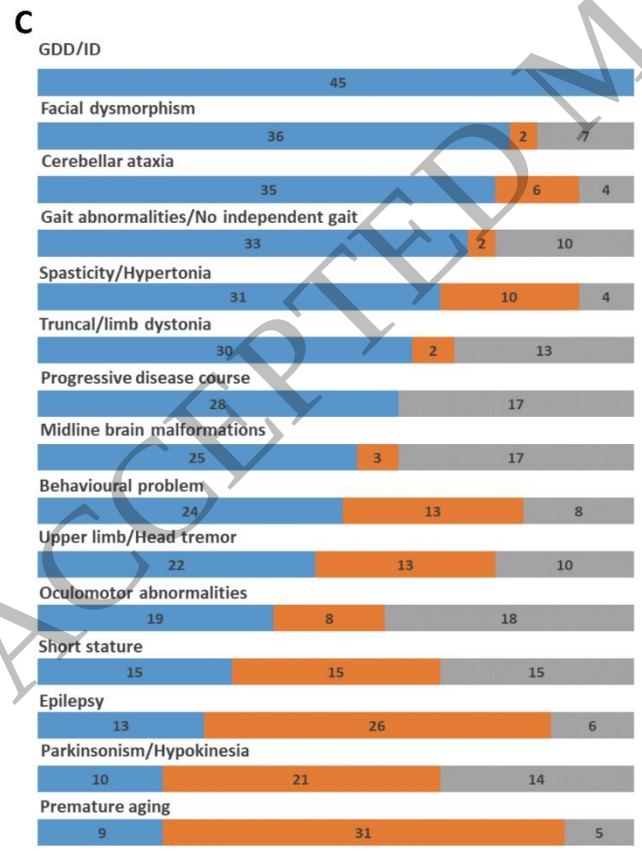

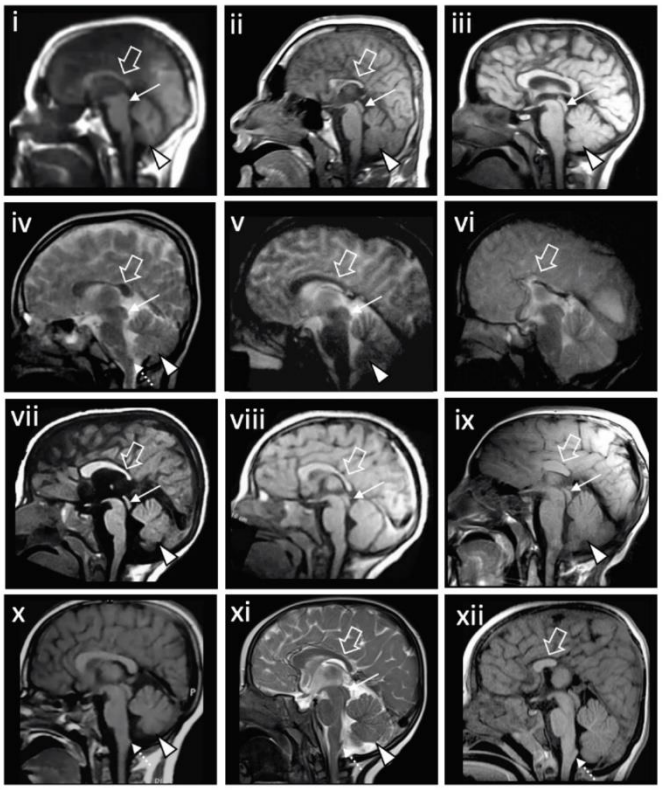

Figure 2
185x230 mm (x DPI)

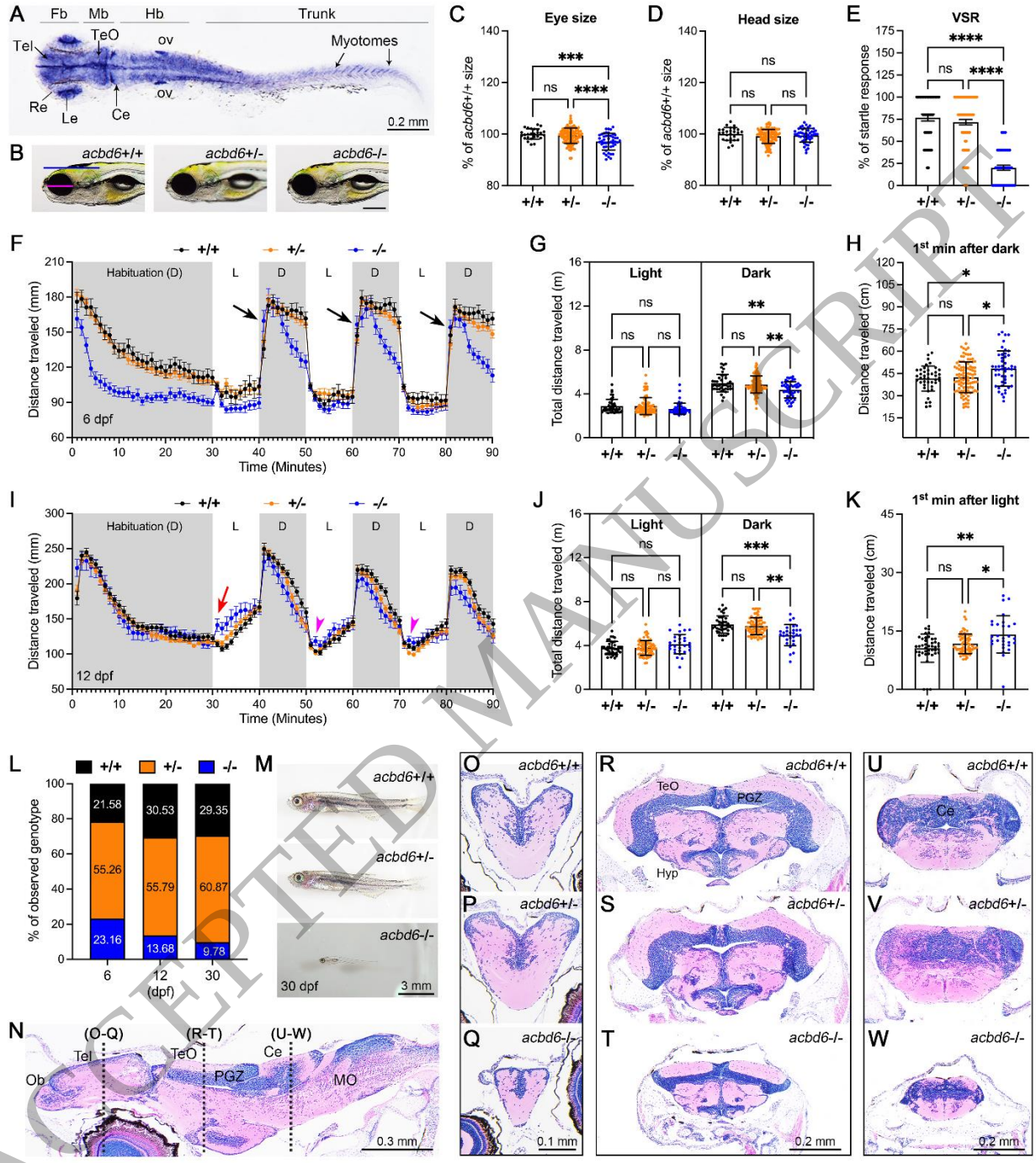

Figure 3
305x344 mm (x DPI)

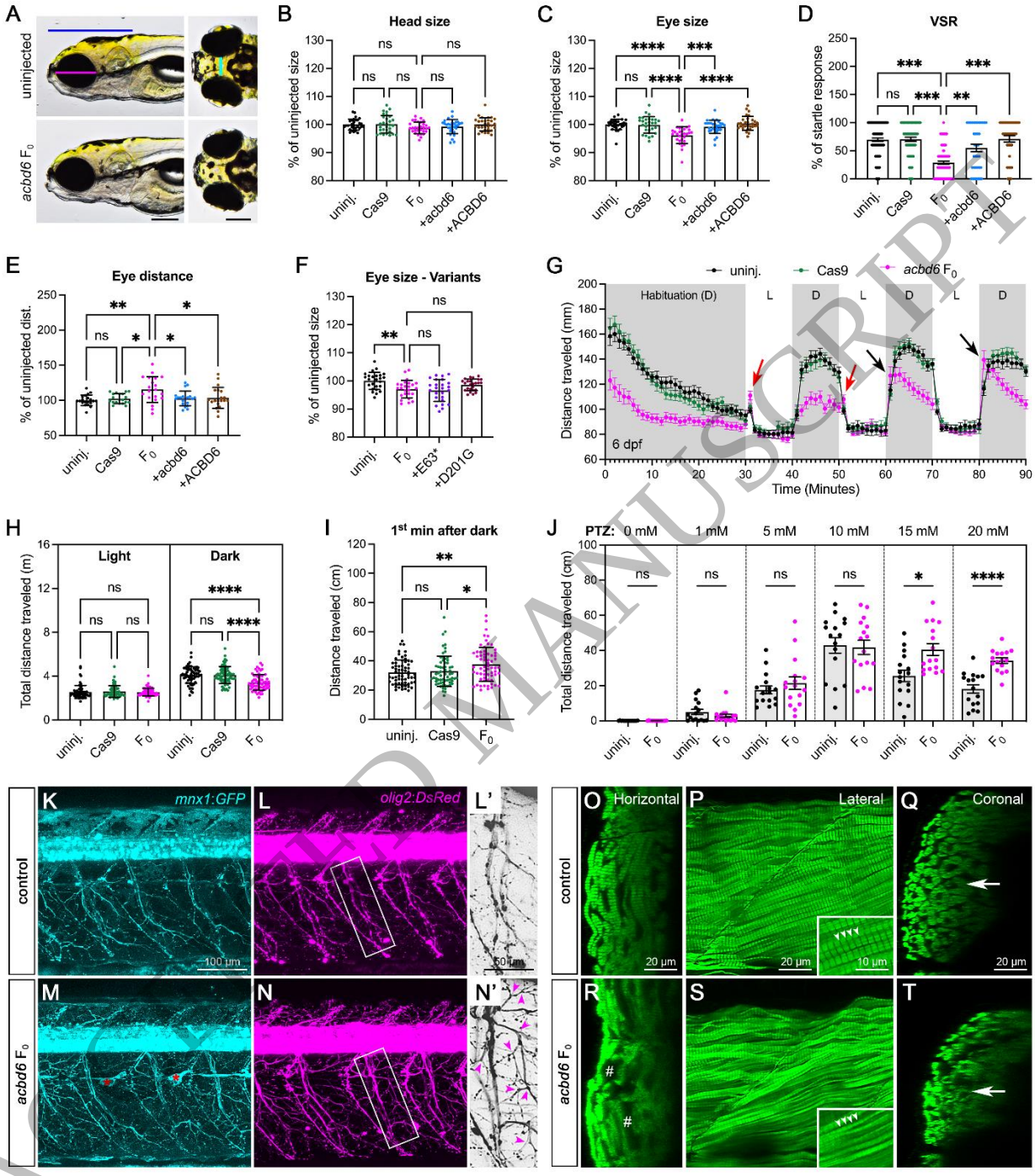

Figure 4
305x345 mm (x DPI)

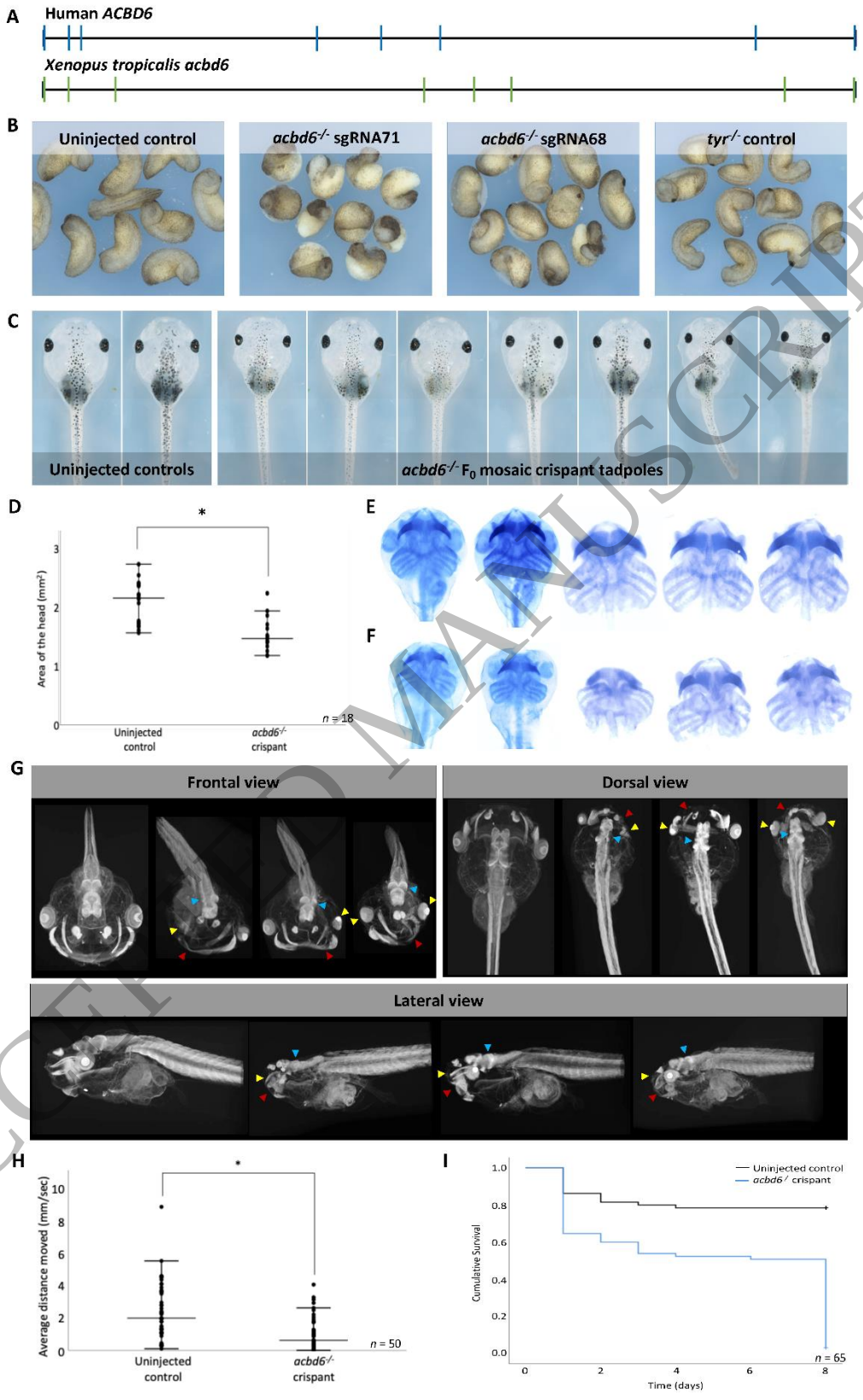

Figure 5
176x275 mm (x DPI)

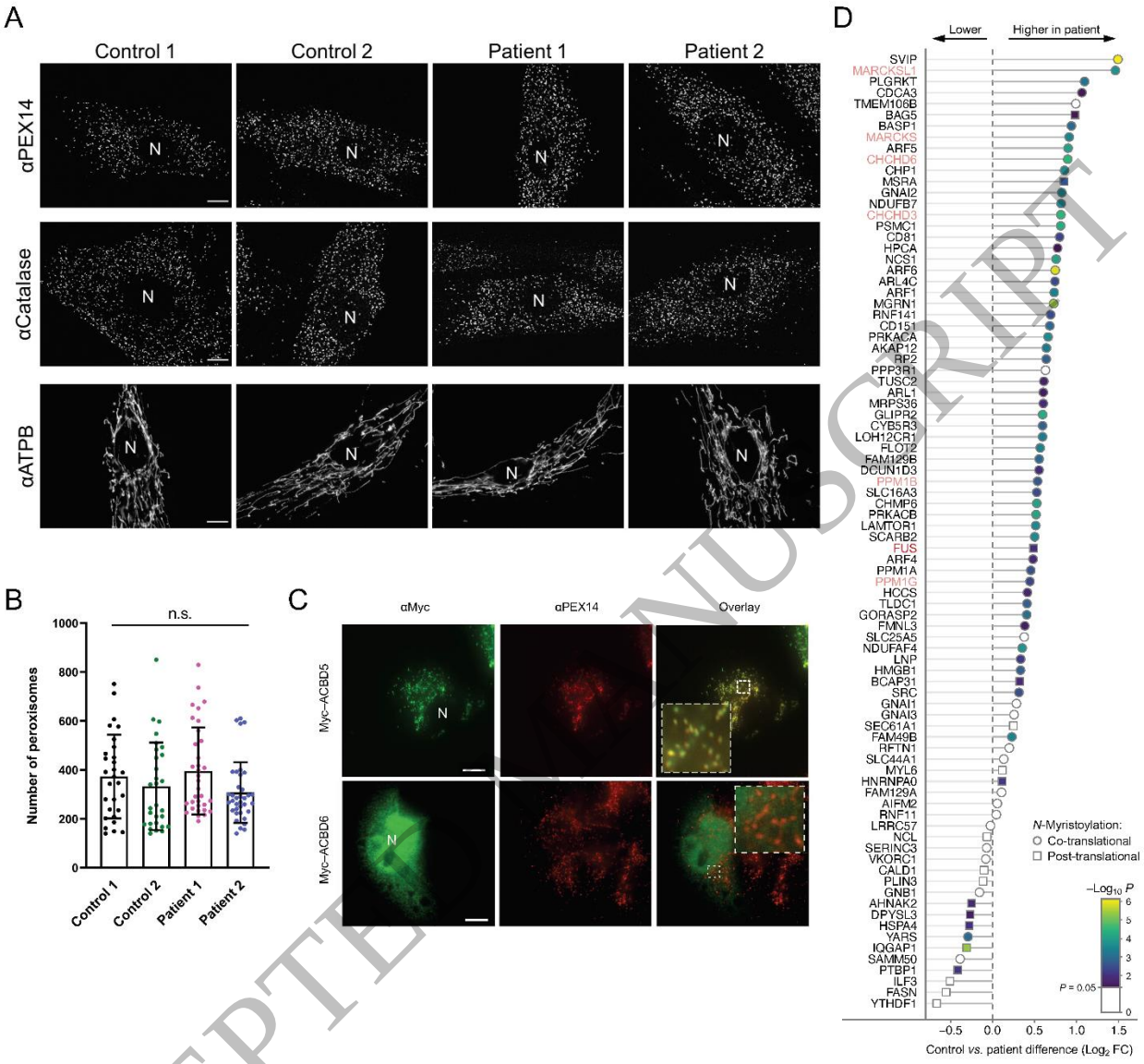

Figure 6
339x316 mm (x DPI)

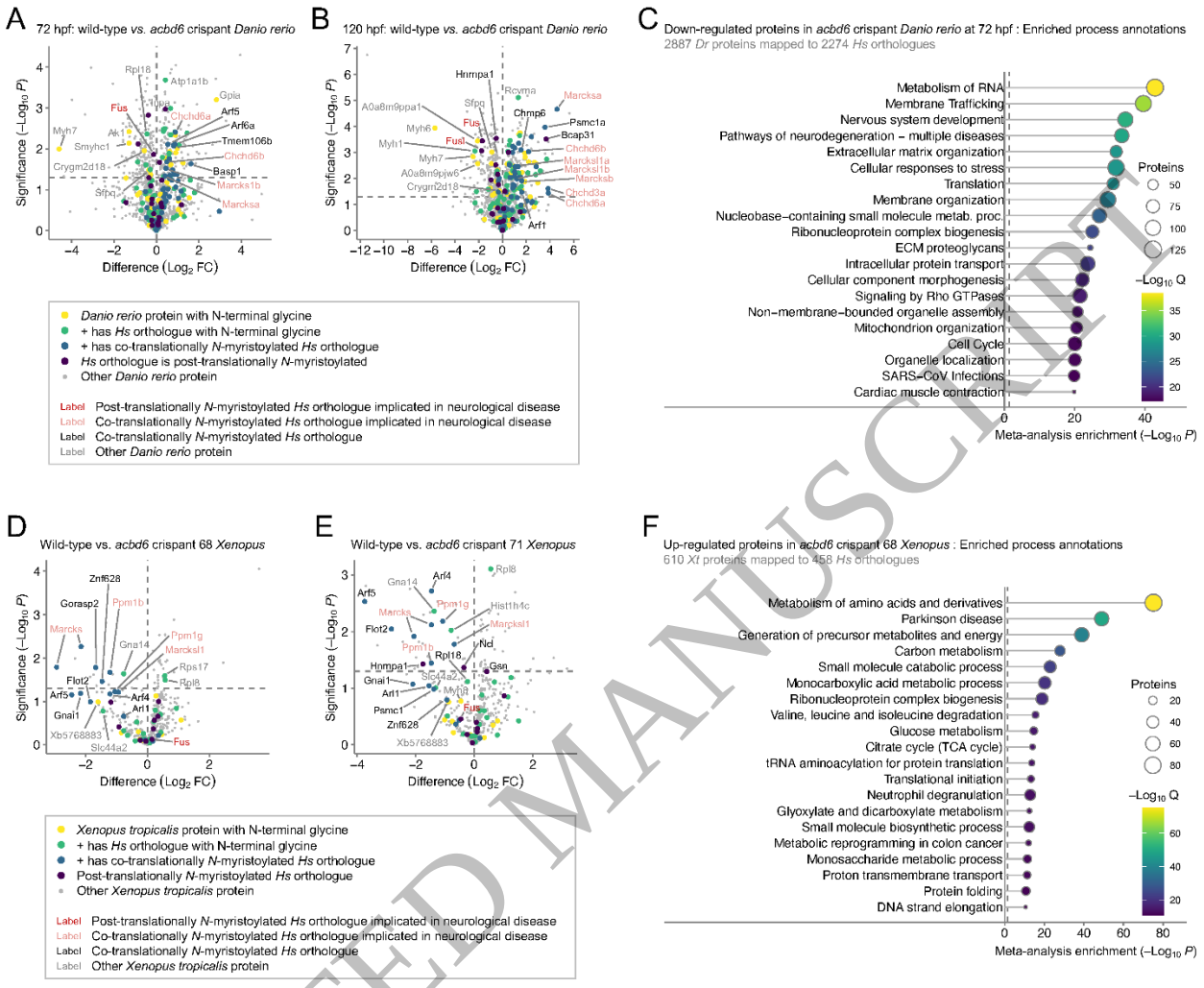

Figure 7
339x283 mm (x DPI)